Study of Information Processing of Phase Pattern in Nonlinear Coupled-Oscillator System

松野, 哲也

https://doi.org/10.11501/3123166

出版情報：九州大学, 1996, 博士（工学）, 論文博士
バージョン：
権利関係：

4 Retrieval Dynamics of Phase Patterns in an Associative Memory System Composed of Coupled Oscillators

This chapter will deal with a rondomly coupled-oscillator system of associative memory. Phase patterns are randomly specified and embedded into coupling parameters so that the system can work as an associative memory system. Retrieval states and macrodynamics of retrieving processes are investigated by a statistical mechanical analysis and numerical simulations.

There are a lot of studies on a neural network model as an associative memory system composed of the linear threshold gates or their modifications.[61, 76-84] Stationary retrieval states in a system of coupled oscillators were already investigated.[85] However, dynamical aspects in the coupled-oscillator system of associative memory have not been analytically studied enough; e.g., there are not any macroscipic equations derived for describing retrieval processes in the system of coupled phase-oscillators. Here, the statistical mechanical analysis is applied to the system to clarify the effects of the storage ratio, the coupling nonlinearity and the natural frequencies on the retrieval dynamics.

The main feature of the model treated in this chapter is that the system has the amplification factor, which is a paremater governing the global coupling nonlinearity (, although the first part of this chapter will deal with the 'weak' nonlinear model without the amplification factor because of the simplicity for studying the basic characteristics of retrieval states and the effects of the natural frequencies on the states). It will be shown that the statistical analysis is fairly available in relatively 'strong' nonlinear regime where the retrieval process is weakly chaotic.

The first part, section 4.1, is concerned with effects of natural frequency distribution on stationary retrieval states in the coupled-oscillator system. The effect of the distribution on the storage capacity is clarified analytically. The effective frequency distribution of the oscillators is also studied. Next, in section 4.2, the dynamics of retrieval processes in a system composed of coupled circle maps is studied by means of a statistical method and numerical simulations. A parameter, which is an amplification factor multiplied to all the coupling strengths, is introduced for investigating the effect of the strength of the coupling nonlinearity on the behavior of the system concerned. The statistical method provides a set of time evolution equations representing the macroscopic behavior. It is shown analytically that the storage capacity is considerably enhanced by the introduced amplification factor. It is also shown that the system exhibits macroscopic chaotic oscillations when the strength of the coupling is sufficiently large. Moreover, the clustering and the chaotic itinerancy are observed, as in other types of the globally coupled nonlinear systems.

4.1 Effects of Distribution of Natural Frequencies on Stationary Retrieval States

Storage capacities were obtained analytically in coupled phase-oscillators without a distribution of natural frequencies.[85] In the coupled-oscillator system concerned here,[86] the natural frequencies of the elementary oscillators are distributed, and coupling coefficients are set so as to make the system work as a phase memory. The distribution of effective frequencies, at which the elements oscillate (the phases rotate), will be analytically described. Note that the continuous-time model is treated only in this section 4.1, while all the other sections concern the discrete-time types.

The model is described as

$$\frac{d\phi_i}{dt} = \omega_i + \sum_{j=1}^{N} K_{ij}\sin(\phi_j - \phi_i + \varphi_{ij}),\ i = 1, \cdots, N, \tag{4.1}$$

where, ϕ_i is a phase of the i-th phase-oscillator, and ω_i is its natural frequency. The natural frequency ω_i is assumed to be a random variable obeying the probability distribution function

$$g(\omega) = \frac{1}{\sqrt{2\pi\gamma^2}}\exp[-\frac{(\omega - \Omega)^2}{2\gamma^2}]. \tag{4.2}$$

The parameter Ω is the central frequency and is chosen to be zero in this study. The p phase patterns are stored in the system by embedding the patterns to the coupling coefficients $\{K_{ij}, \varphi_{ij}\}$ as

$$K_{ij}\exp(\mathrm{i}\varphi_{ij}) = \frac{1}{N}\sum_{\mu=1}^{p}\exp[\mathrm{i}(\theta_i^\mu - \theta_j^\mu)],\ i, j = 1, \cdots, N, \tag{4.3}$$

where θ_i^μ is the i-th component of the μ-th phase pattern to be memorized. The memorized phase patterns are determined randomly.[86] A schematic illustration for the system concerned in this chapter is shown in Fig. 4.1. The overlap m^μ, which is representing the similarity between the phase configuration of the system and the μ-th memorized phase pattern, is defined as

$$m^\mu = \frac{1}{N}\sum_{j=1}^{N}\exp[\mathrm{i}(\phi_j - \theta_j^\mu)],\ \mu = 1, \cdots, p. \tag{4.4}$$

Let us consider the situation in which the first memorized phase pattern is retrieved (m^1 is of order $O(1)$). Due to the distribution of the natural frequencies, the overlap $m^1(t)$ oscillates. Let m be an averaged value of $m^1(t)$ with respect to time. Using the self-consistent signal-to-noise analysis (SCSNA) method developed by Shiino and Fukai,[83] we can determine analytically the storage capacity under the distribution of natural frequencies (see Appendix C·1). It should be noted that the natural frequencies and the memorized phase patterns are assumed

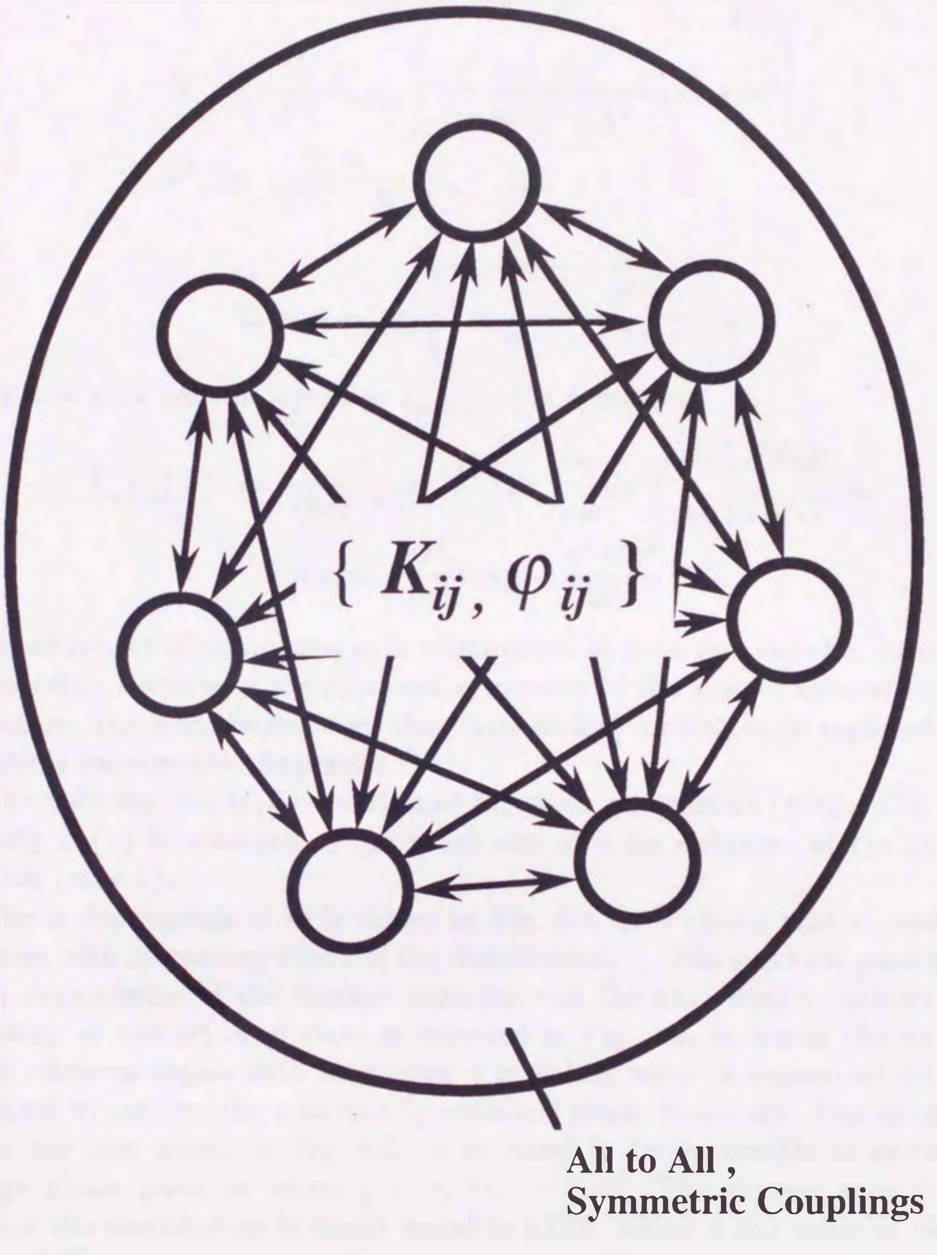

Fig. 4.1: Schematic illustration of the structure of the coupled-oscillator system concerned in this chapter. Randomly specified phase patterns are embedded into the coupling parameters $\{K_{ij}; \varphi_{ij}\}$.

to be statistically independent of each other. We can derive a set of equations describing the macroscopic stationary state as

$$m = \widehat{I}_{m,\tilde{\sigma},\gamma}\left[\frac{x+1}{\sqrt{(x+1)^2+y^2}}h_m(x,y,\omega)\right], \tag{4.5}$$

$$M = \frac{1}{2\tilde{\sigma}^2}\widehat{I}_{m,\tilde{\sigma},\gamma}\left[\frac{x^2+x+y^2}{\sqrt{(x+1)^2+y^2}}h_m(x,y,\omega)\right], \tag{4.6}$$

$$\tilde{\sigma}^2 = \frac{\alpha}{2(m-M)^2}\widehat{I}_{m,\tilde{\sigma},\gamma}[1], \tag{4.7}$$

with

$$h_m(x,y,\omega) = \sqrt{1-\frac{\omega^2}{m^2[(x+1)^2+y^2]}}, \tag{4.8}$$

where $\alpha = p/N$ and the operator $\widehat{I}_{m,\tilde{\sigma},\gamma}[\,\cdot\,]$ is defined as

$$\widehat{I}_{m,\tilde{\sigma},\gamma}[\,\cdot\,] = \frac{1}{(2\pi)^{3/2}\gamma\tilde{\sigma}^2}\int_{-\infty}^{\infty}dx\int_{-\infty}^{\infty}dy\int_{-m\sqrt{(x+1)^2+y^2}}^{m\sqrt{(x+1)^2+y^2}}d\omega \times \exp(-\frac{\omega^2}{2\gamma^2})\exp(-\frac{x^2+y^2}{2\tilde{\sigma}^2})[\,\cdot\,]. \tag{4.9}$$

In the above set of equations, m is constrained to be a real variable without loss of generality because of the rotaional symmetry of the system concerned. In the derivation, the summation over the phase-locked oscillators is replaced by the statistical average (see Appendix C·1).

The solution $(m, M, \tilde{\sigma})$ is obtained for given parameters (γ, α). The storage capacity $\alpha_c(\gamma)$ is obtained as the maximum of α for existence of the nontrivial solution $(m \neq 0)$.

The α dependence of m is shown in Fig. 4.2. It is shown that α_c and $m(\alpha_c)$ decrease with increasing width of the distribution, γ. The state diagram showing the γ dependence of the storage capacity and the analytically obtained phase boundary of the retrieval state is depicted in Fig. 4.3, in which the narrowing of the retrieval region with increasing γ is clearly seen. A numerical simulation was done to confirm the analytically obtained phase boundary. The investigated points are also shown in Fig. 4.3. It is found to be impossible to retrieve any storage phase patterns when $\gamma > \gamma_c$ ($\gamma_c \sim 0.6$). The storage capacity $\alpha_c(0)$ without the distribution is nearly equal to 0.038, which is the same as the value reported.[85)]

The analytical expression of the effective frequency distribution is also found, which represents the oscillatory dynamics of the overlap $|m^1(t)|$ (see Appendix C·2). Let $G(\tilde{\omega})$ be the distribution function, which can be decomposed into the phase-locked part and the unlocked part as $G(\tilde{\omega}) = G_S(\tilde{\omega}) + G_D(\tilde{\omega})$. The distribution of the effective frequency $\tilde{\omega}$ of the unlocked oscillators is expressed as

$$G_D(\tilde{\omega}) = E[g(\omega)\left|\frac{d\omega}{d\tilde{\omega}}\right|], \tag{4.10}$$

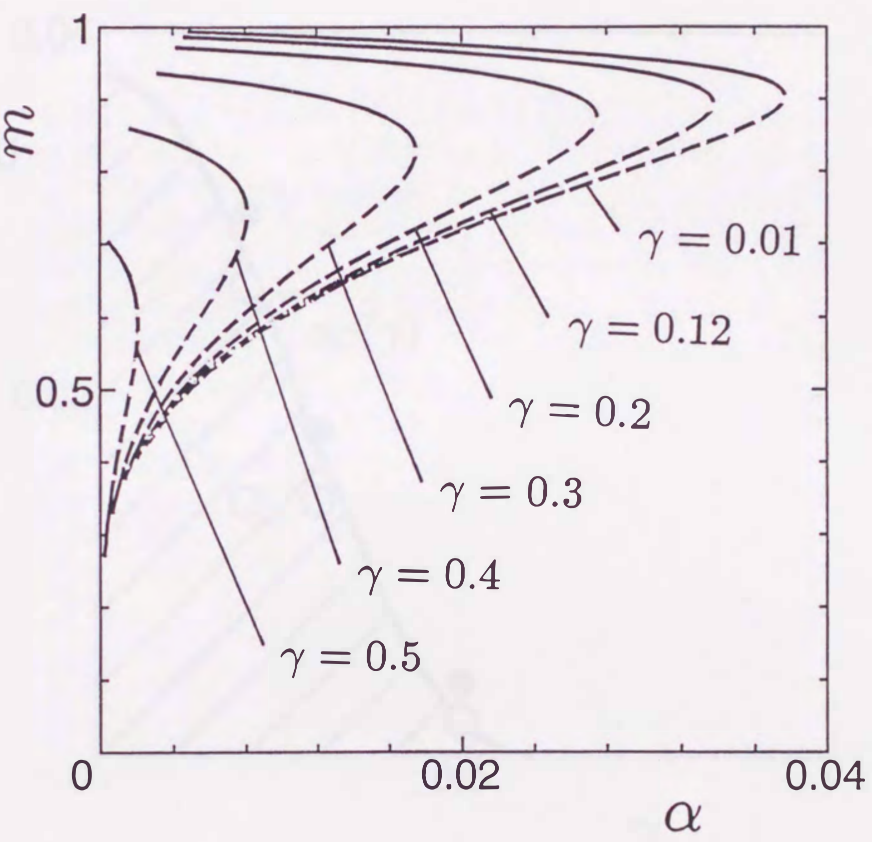

Fig. 4.2: The memory rate α dependences of the nonzero solutions of the overlaps m at various widths γ of the distribution of the natural frequency. Solid lines correspond to the stable equilibrium state positions, while dashed ones do not.

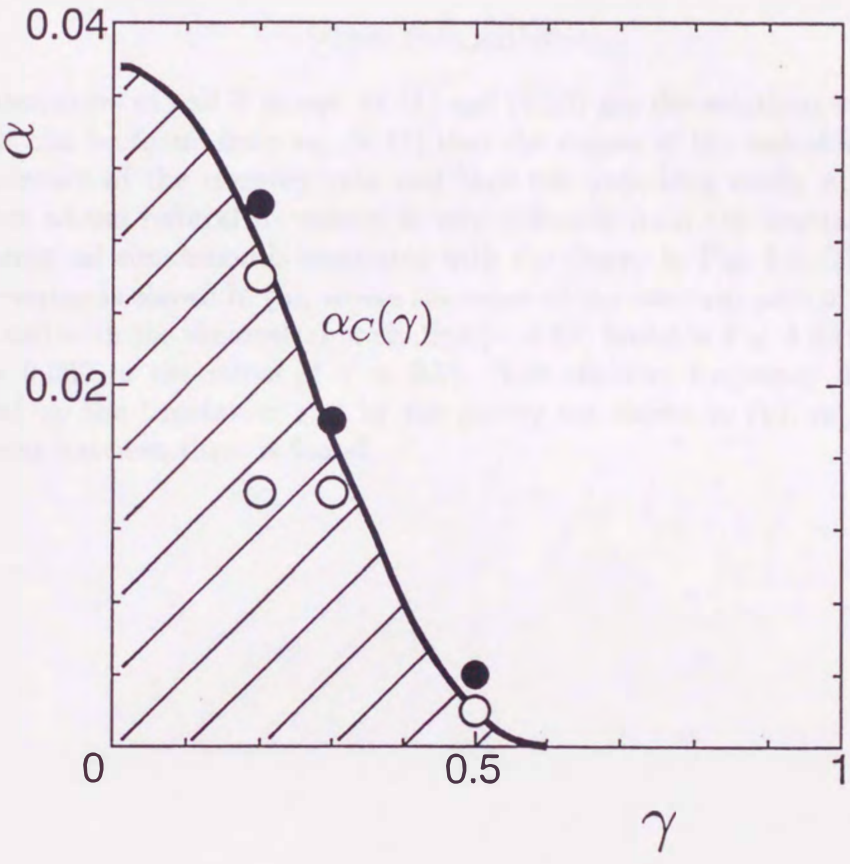

Fig. 4.3: The state diagram in the γ-α plane. The shaded area under the analytically obtained phase boundary $\alpha_c(\gamma)$ is the retrieval region. Open and closed circles denote successes and failures in the numerically simulated retrievals, respectively. The number of oscillators used in the simulation is 500.

where $E[\,\cdot\,]$ denotes expectation. We finally obtain the following expression by calculating the statistical average (see Appendix C·2):

$$\begin{aligned} G_D(\tilde{\omega}) &= \frac{1}{(2\pi)^{3/2}\tilde{\sigma}^2\gamma}\int_0^\infty dR\int_0^{2\pi} d\theta\,\frac{R|\tilde{\omega}|}{\sqrt{\tilde{\omega}^2+m^2R^2}} \\ &\quad \times\exp\Big(-\frac{R^2-2R\cos\theta+1}{2\tilde{\sigma}^2}\Big)\exp\Big(-\frac{\tilde{\omega}^2+m^2R^2}{2\gamma^2}\Big). \end{aligned} \tag{4.11}$$

The locked part is expressed as

$$G_S(\tilde{\omega}) = \hat{I}_{m,\tilde{\sigma},\gamma}[1]\delta(\tilde{\omega}). \tag{4.12}$$

The parameters m and $\tilde{\sigma}$ in eqs. (4.11) and (4.12) are the solutions of eqs. (4.5)-(4.7). It can be found from eq. (4.11) that the degree of the unlocking increases with increase of the memory rate and that the unlocking easily occurs at the oscillator whose natural frequency is very different from the central frequency. The numerical simulation is compared with the theory in Fig. 4.4. The behavior of the overlap is shown in (a), where the value of the constant part of the overlap agrees well with the theoretical prediction (~ 0.62) found in Fig. 4.2 (the position of $\alpha = 0.002$ in the curve of $\gamma = 0.5$). The effective frequency distributions obtained by the simulation and by the theory are shown in (b), in which good agreement between them is found.

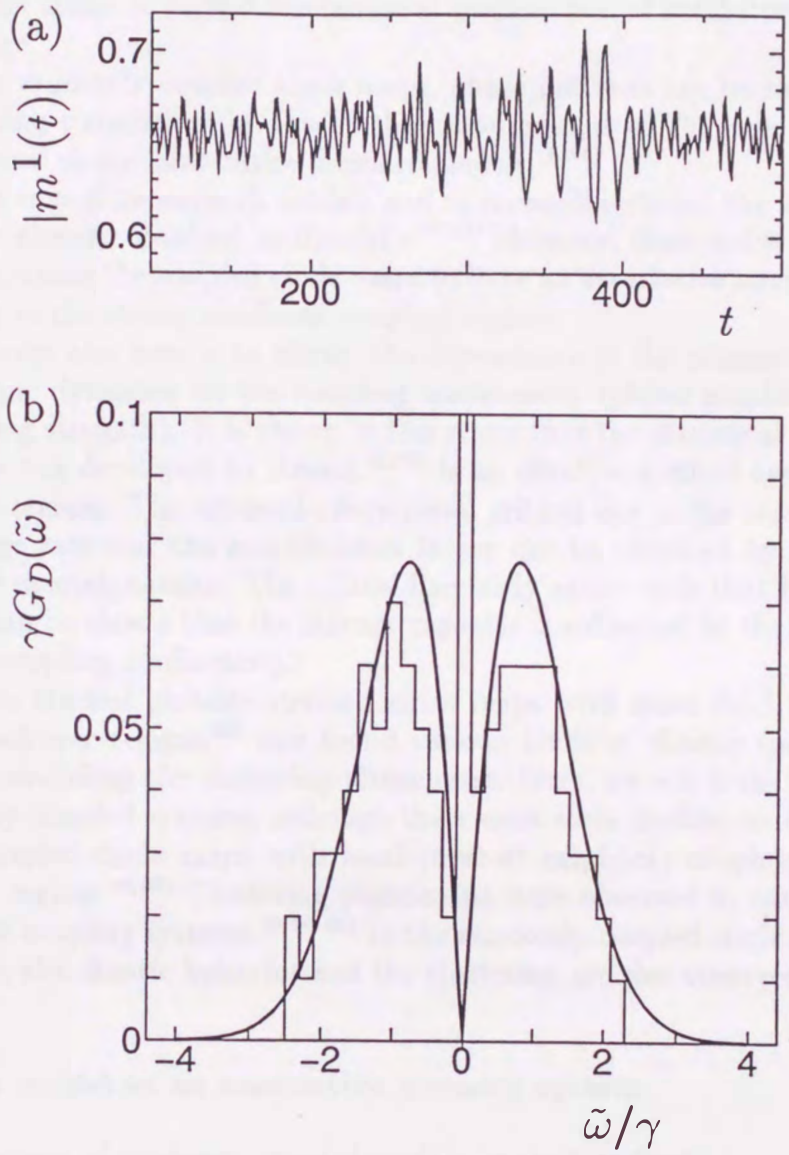

Fig. 4.4: (a) The oscillation of the overlap. (b) The analytically calculated curve (thick solid line) of the effective frequency distribution of the unlocked part and the numerically calculated histogram of the distribution. The parameters in the numerical simulation are as follows: $\gamma = 0.5$, $\alpha = 0.002$, $N = 500$.

4.2 Neurodynamics in Randomly Coupled Circle Maps

We will concern a system of coupled circle maps as a natural or intuitive extension of a single circle map to describe coupled oscillatory systems.[87] The aim of this study is to find fundamental mechanisms of oscillatory information processings.

In the randomly coupled circle maps, phase patterns can be memorized into the coupling parameters in almost the same manner as the rule often used in other typical neural associative memory models.[76-84]

In the spin-glass network models and in its modifications, the storage capacities were already obtained analytically.[76-84] However, there exists no analytical work concerning the coupled circle maps to have an associative memory function, especially in the strong nonlinear coupling regime.

The main aim here is to clarify the dependence of the storage capacity and macroscopic dynamics on the coupling nonlinearity (global amplification factor for coupling strength). It is shown in this study that the statistical neurodynamics, which was developed by Amari,[61,78] is an effective method even in a strong nonlinear regime. The retrieval-nonretrieval critical line in the state diagram of the storage rate and the amplification factor can be obtained by means of the statistical neurodynamics. The critical line fairly agrees with that found numerically. It can be shown that the storage capacity is enhanced by the amplification factor of coupling nonlinearity.

Kaneko studied globally coupled circle maps with mean field coupling in a strong nonlinear regime,[63] and found various kinds of chaotic spatio-temporal dynamics including the clustering phenomena. Here, we will focus our attention on globally coupled systems, although there exist some studies concerning a system of coupled circle maps with local (nearest neighbor) coupling in a strong nonlinear regime.[88,89] Clustering phenomena were observed in various kinds of mean-field coupling systems.[59,90-95] In the randomly coupled circle maps used in this study, the chaotic behavior and the clustering are also observed.

4.2.1 A model as an associative memory system

The system of randomly coupled circle maps is described by a set of discrete-time evolution equations of phases of the elementary oscillators as follows:

$$\begin{aligned} \phi_i(t+1) &= \phi_i(t) + \omega_i + \beta \sum_{j=1}^{N} K_{ij} \sin(\phi_j(t) - \phi_i(t) + \varphi_{ij}), \\ & \quad i = 1, \cdots, N, \end{aligned} \tag{4.13}$$

where $\phi_i(t)$ is the phase of the i-th element at the discrete time t (t: integer). The parameter ω_i is a natural frequency of the i-th elementary oscillator. Here, let us consider the case of $\omega_i = 0$ for $i = 1, \cdots, N$. The coupling paramaters K_{ij} and φ_{ij} are determined so as to make the system work as an associative memory machine:

$$K_{ij}\exp(\mathrm{i}\varphi_{ij}) = \frac{1}{N}\sum_{\mu=1}^{p}\exp[\mathrm{i}(\theta_i^\mu - \theta_j^\mu)],\ i,j = 1,\cdots,N, \tag{4.14}$$

where θ_i^μ is the i-th component of the μ-th embedded phase pattern. The parameter β is an amplification factor of the coupling strength in eq. (4.13).

The storage rate α is defined as the number p of the embedded patterns normalized by the system size N, i.e., $\alpha = p/N$. The phase patterns $\boldsymbol{\theta}^\mu = (\theta_1^\mu,\cdots,\theta_N^\mu)$, $\mu = 1,\cdots,p$, are randomly determined and fixed.

The model described by eq. (4.13) is a discrete-time version of the model (eq. (4.1)) concerned in the previous section. It should be noted that the dynamical behavior in the discrete-time model is quite different from that in the continuous-time model especially in the case of strong nonlinearity (β being considerably large).

4.2.2 Time evolution equations of macroscopic variables

We will derive macroscopic time evolution equations by means of the statistical neurodynamics.[61,78] A macroscopic variable, the overlap $m^\mu(t)$, reflecting the degree of retrieval of the μ-th embedded phase pattern is introduced as

$$m^\mu(t) = \frac{1}{N}\sum_{i=1}^{N}\exp[\mathrm{i}(\phi_i(t) - \theta_i^\mu)],\ \mu = 1,\cdots,p. \tag{4.15}$$

Let us consider the retrieval of the 1-st pattern $\{\theta_i^1\}$ and assume that $|m^1(t)|$ is of order $O(1)$ and $|m^\mu(t)|$ is of order $O(1/\sqrt{N})$ for $\mu \neq 1$. Without losing generality, we can assume as $\theta_i^1 = 0$ for $i = 1,\cdots,N$. Hence, the macroscopic variable $m^1(t)$, to which will be referred simply as $m(t)$, is expressed as

$$m(t) = \frac{1}{N}\sum_{i=1}^{N}\exp[\mathrm{i}\phi_i(t)]. \tag{4.16}$$

The macroscopic variable $m(t)$ can be assumed to be a real variable without loss of generality because of a rotational symmetry in the system concerned.

By substituting eq. (4.14) into eq. (4.13), we obtain

$$\phi_i(t+1) = \phi_i(t) + \beta\ \mathrm{Im}\{\exp[-\mathrm{i}\phi_i(t)][m(t) + Z_i(t)]\}, \tag{4.17}$$

where

$$Z_i(t) = \frac{1}{N}{\sum_\mu}'{\sum_j}'\exp\{\mathrm{i}[\phi_j(t) + \theta_i^\mu - \theta_j^\mu]\}. \tag{4.18}$$

The symbol ${\sum_\mu}'$ denotes the summation over $\mu \neq 1$, and ${\sum_j}'$ denotes the summation over $j \neq i$.

The term $Z_i(t)$ can be considered as a random variable. By the central limit theorem, $Z_i(t)$ can be regarded as normally distributed with

$$E[Z_i(t)] = 0,\quad E[|Z_i(t)|^2] = 2\sigma^2(t), \tag{4.19}$$

where $E[\ \cdot\ ]$ denotes the expectation, and $\sigma^2(t)$ is the variance of the real or imaginary part of the random variable $Z_i(t)$. Moreover, $Z_i(t)$ and $Z_j(t)$ can be assumed to be statistically independent of each other when $i \neq j$:

$$E[Z_i(t)Z_j^*(t)] = 0, \quad i \neq j. \tag{4.20}$$

For the law of large numbers, eq. (4.16) can be rewritten as

$$m(t) = E[\exp[\mathrm{i}\phi_i(t)]]. \tag{4.21}$$

Hence, the time evolution equation for $m(t)$ is easily obtained as

$$\begin{aligned} m(t+1) &= E[\exp[\mathrm{i}\phi_i(t)]\exp\{\mathrm{i}\beta\mathrm{Im}\{\exp[-\mathrm{i}\phi_i(t)][m(t)+Z_i(t)]\}\}] \\ &= e^{-\beta^2\sigma^2(t)/2}F_\beta[m(t)], \end{aligned} \tag{4.22}$$

where

$$F_\beta(m) = E[\exp[\mathrm{i}(\phi_i - \beta m \sin\phi_i)]]. \tag{4.23}$$

In the above, it should be noted that we used the assumption that $\phi_i(t)$ and $Z_i(t)$ are statistically independent of each other. However, there exists a higher order correlation between them. The correlation has to be taken into account for calculating $\sigma^2(t)$, as explained in Appendix C·4.

The explicit expression of $F_\beta(m)$ can be obtained analytically by an assumption that the phases are unimodally distributed as expressed by the following probability density function:

$$\rho_m(\phi) = \frac{1}{2\pi I_0(a)}\exp(a\cos\phi), \tag{4.24}$$

where a parameter a $(= a(m))$ is defined so as to satisfy

$$m = I_1(a)/I_0(a). \tag{4.25}$$

The functions $I_0(\cdot)$ and $I_1(\cdot)$ are the modified Bessel functions of the zero-th and the 1-st order, respectively. The assumed probability density function eq. (4.24) is consistent with the condition eq. (4.21). The obtained analytical expression for $F_\beta(m)$ is

$$F_\beta(m) = \frac{\sqrt{a+b}}{\sqrt{a-b}}\frac{I_1(\sqrt{a^2-b^2})}{I_0(a)}, \tag{4.26}$$

where $b = \beta m$. The derivation of eq. (4.26) is shown in Appendix C·3.

We can also obtain analytically the time evolution equation for $\sigma^2(t)$ by means of the statistical neurodynamics, as shown in Appendix C·4. The obtained set of time evolution equations of the macroscopic variables $m(t)$ and $\sigma^2(t)$ are expressed as

$$m(t+1) = e^{-\beta^2\sigma^2(t)/2}F_\beta[m(t)], \tag{4.27}$$

$$\begin{aligned} \sigma^2(t+1) = \frac{\alpha}{2} + e^{-\beta^2\sigma^2(t)}\{&2G_\beta^2[m(t)]\sigma^4(t) \\ &+(F_\beta'^2[m(t)] + G_\beta^2[m(t)])\sigma^2(t) \\ &+\frac{1}{2}\alpha\beta G_\beta^2[m(t)]\}, \end{aligned} \tag{4.28}$$

where $\sigma^2(0) = \alpha/2$, and the prime means differentiation with respect to m. The function $G_\beta(m)$ is given as (see Appendix C·3)

$$G_\beta(m) = \frac{I_0(\sqrt{a^2 - b^2})}{I_0(a)}. \tag{4.29}$$

The functions $F_\beta(m)$ and $G_\beta(m)$ are shown in Fig. 4.5. It can be seen that the nonlinearity of the macroscopic dynamics increases by increasing β. The nonlinearity can be expected to induce oscillatory macrodynamics. However, the analytical consideration here cannot describe oscillatory dynamics, as will be discussed in later sections.

A typical retrieval dynamics in the relatively weak nonlinear regime is shown in Fig. 4.6(a), in which time evolutions of the macroscopic variable $m(t)$ is drawn with various initial conditions by using the analytically obtained set of eqs. (4.27) and (4.28). In the case of Fig. 4.6(a) where α is sufficiently small, the system can retrieve an embedded pattern when the initial phase configuration is sufficiently close or similar to the corresponding pattern (when $m(0)$ is larger than a threshold value m_h). However, the system cannot retrieve an embedded pattern when $m(0) < m_\mathrm{h}$.

Figure 4.6(b) shows the orbits of the retrieval processes in the $m - \sigma^2$ space. There are three equilibrium points in the state space. A point which has the largest value of m (say, m_a) and a point which has the zero value of m are stable, while the one between them is unstable. A variable $m(t)$ converges to m_a in the case of (successful) retrieval, whereas it converges to zero in the case of nonretrieval. The threshold value m_h can be found by going back to the initial point $(m(0), \sigma^2(0))$ over a path which is connecting to the unstable point.

The spin-glass network models[61, 78, 80, 83] also have the characteristics mentioned above. In other words, the system of randomly coupled circle maps is basically similar to the spin-glass models. It should be noted, however, that the amplification factor β is specific for the system of coupled circle maps studied here. That is, a corresponding parameter does not exist in the spin-glass network models. The parameter β looks apparently similar to what is called a gain in spin-glass network models. However, the inverse of the gain corresponds to the width of the natural frequency distribution in the system concerned here, although the width is set to zero in this study. When β is relatively large, the parameter causes oscillatory and chaotic dynamics, as will be mentioned in later sections.

4.2.3 Retrieval-nonretrieval critical line

The system concerened here can retrieve any embedded pattern when the storage rate α is smaller than the certain critical value α_c. The critical value α_c is called the storage capacity, which is dependent on the parameter β.

In this section, we will obtain the coupling nonlinearity amplification factor β dependence of the storage capacity $\alpha_\mathrm{c}(\beta)$, which is the retrieval-nonretrieval critical line in the $\alpha - \beta$ plain.

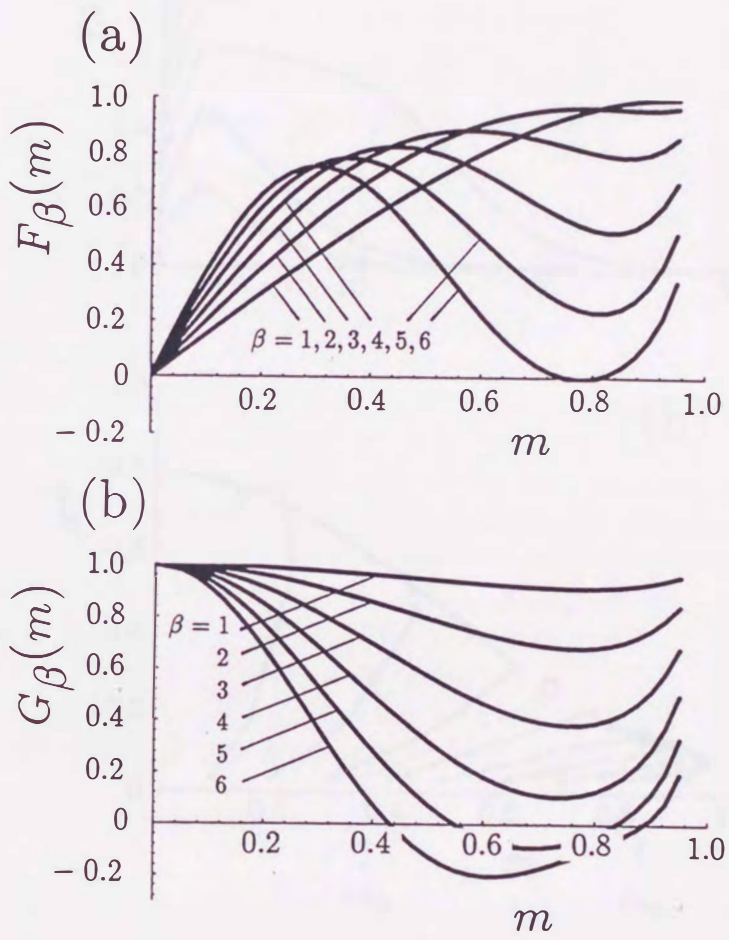

Fig. 4.5: Functions of (a) $F_\beta(m)$ and (b) $G_\beta(m)$.

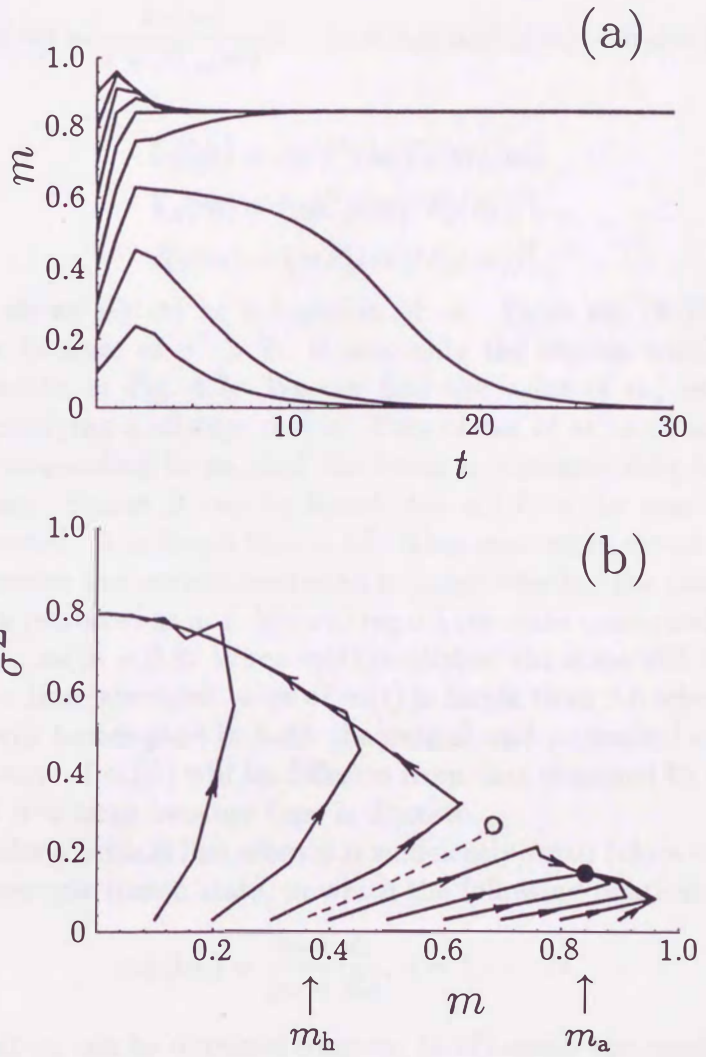

Fig. 4.6: Behaviour of macroscopic variables with various initial conditions. $\alpha = 0.06$ and $\beta = 1.5$. (a) Dynamics of $m(t)$, (b) orbits of retrieval processes in the m–σ^2 space.

Let us concern the simple stationary macroscopic state, which means that $(m(t+1), \sigma^2(t+1)) = (m(t), \sigma^2(t))$. A relation

$$e^{-\beta^2\sigma^2} = (m/F_\beta(m))^2 \tag{4.30}$$

is obtained from eq. (4.27). By using the above relation and eq. (4.28), we can find dependences of α on m and β, given by $\alpha = \tilde{\alpha}_\beta(m)$, where

$$\tilde{\alpha}_\beta(m) = \frac{L_\beta(m)}{1+\beta\Gamma_\beta(m)}[1-(1+L_\beta(m))\Gamma_\beta(m) - H_\beta(m)], \tag{4.31}$$

with

$$L_\beta(m) = (4/\beta^2)\ln[F_\beta(m)/m], \tag{4.32}$$

$$\Gamma_\beta(m) = (mG_\beta(m)/F_\beta(m))^2, \tag{4.33}$$

$$H_\beta(m) = (mF'_\beta(m)/F_\beta(m))^2. \tag{4.34}$$

Figure 4.7 shows $\tilde{\alpha}_\beta(m)$ as a function of m. From eq. (4.30), it is found as $F_\beta(m) > m$ because of $\sigma^2 > 0$. Hence, only the regime which suffices this condition is plotted in Fig. 4.7. We can find the value of m_a on a curve of a certain β by specifying a storage rate α. Two values of m are found, larger one of which is corresponding to m_a and the other is corresponding to an unstable equilibrium point. Hence, it can be found that $\alpha_c(\beta)$ is the maximum value of the curve concerned. It is found that $\alpha_c(\beta)$ takes maximum around $\beta = 2.5$.

Let us determine the retrieval criterion to judge whether the concerning memorized pattern is retrieved or not. We will regard the state concerned as 'retrieved' if $m_a > 0.5$ when $m(0) = 0.9$. When $m(t)$ oscillates, the state will be regarded as 'retrieved' if the time averaged value of $m(t)$ is larger than 0.5 when $m(0) = 0.9$. The criterion will be adopted in both theoretical and numerical considerations. Note that the value of $\alpha_c(\beta)$ will be different from that obtained by the maximum of $\tilde{\alpha}_\beta(m)$ when β is large because time is discrete.

Let us consider a critical line when β is sufficiently small (close to zero). There exists the microscopic frozen state, in which the following relation holds:

$$\exp(i\phi_i) = \frac{m+Z_i}{|m+Z_i|}, \quad i = 1, \cdots, N. \tag{4.35}$$

The above equation can be obtained from eq. (4.17) under the condition of $\phi_i(t+1) = \phi_i(t)$ for $i = 1, \cdots, N$. The solution which satisfies eq. (4.35) does not exist above the line of $\alpha = 0.038$.[85,86] It can be expected that the frozen state destabilizes when β is sufficiently large. Indeed, in the numerical simulation, $m(t)$ oscillates or the clustering phenomenon is observed in the large β regime.

4.2.4 Retrieval processes

Figure 4.8 shows typical examples of retrieval processes in a relatively weak nonlinear (relatively small β) regime. The retrieval processes in (a) fairly well reproduces the theoretical prediction depicted in Fig. 4.6(a). Actually, numerically

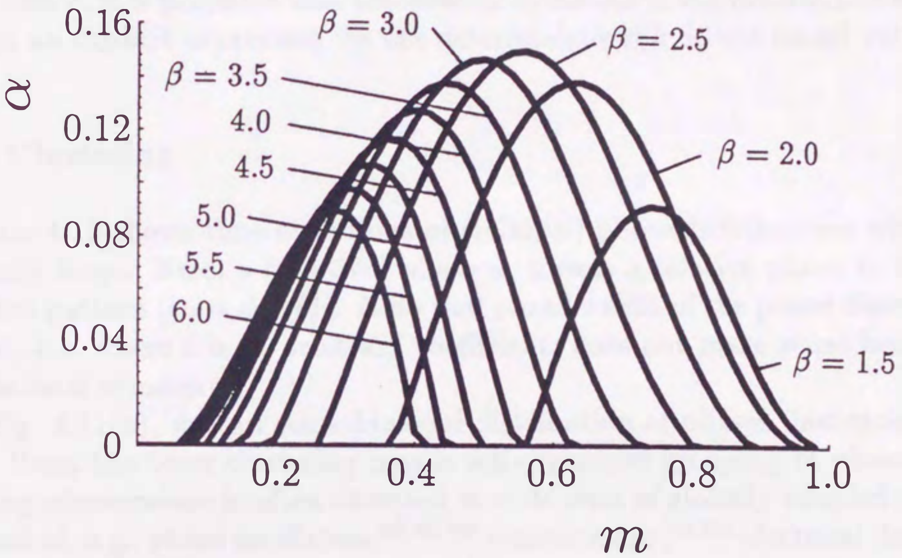

Fig. 4.7: Plots of $\tilde{\alpha}_\beta(m)$ with various values of β.

obtained m_a is slightly larger than that obtained analytically. A response speed numerically observed could be slightly slower than that predicted analytically.

Figure 4.9 shows an example of oscillatory retrieval processes observed in a relatively strong nonlinear (relatively large β) regime. The oscillation is not a transient but a stationary phenomenon. In this case of Fig. 4.9, the oscillation is chaotic, which could be a high dimensional deterministic chaos. In spite of chaotic $m(t)$, the successful retrieval is achieved when $m(0)$ is sufficiently large. Averagingly, $m(t)$ takes a value which is of order $O(1)$ in this case.

Figure 4.10 shows return maps of $m(t)$ in the cases of chaotic oscillations. Scattered points over a certain area in the $m(t)$-$m(t+1)$ indicate the chaotic oscillation. The cloud of the distributed points may be a projection of a high dimensional attractor. The chaotic dynamics may be a fluctuation due to a finite size effect. We investigated at N=200, 400, 500 and 700. However, differences of amplitudes of oscillations in these cases (with the same parameters) were not found. Hence, it is plausible that the chaotic dynamics is the deterministic chaos, although an explicit expression for the deterministic rule is not found yet.

4.2.5 Clustering

Figure 4.11 shows time evolutions of (relative) phase distributions when β is sufficiently large. Here, a (relative) phase ψ_i means a relative phase to the 1-st embedded pattern ($\psi_i = \phi_i - \theta_i^1$). Note that parallel shift of the phase distribution ($\psi_i \rightarrow \psi_i + c$, where c is an arbitrary coefficient) does not make sense because of the rotational symmetry.

In Fig. 4.11(a), we can see a bimodal distribution of phases, indicating clustering. Here, the term clustering means self-organized grouping of phases. The clustering phenomenon is often observed in wide class of globally coupled systems composed of, e.g., phase oscillators,[59, 93, 94] chaotic maps,[90, 91] electrical devices[92] and biological cells.[95] In this study, two clusters, which are almost the same size (we will use the term 2-cluster state to refer to this state), are observed in a certain area (indicated by a dashed line in the state diagram shown in Fig. 4.12). Each cluster has a relatively broad distribution.

Let us consider the case of $\beta = 2.5$, and regard α as a bifurcation parameter. The 2-cluster state degrades by increasing α, as can be seen from Figs. 4.11(a) and 4.11(b). Moreover, a unimodal distribution (with a slight fluctuation) realizes when α is sufficiently large (as shown in Fig. 4.11(c)). When $\alpha > \alpha_c$, a homogeneous distribution emerges (Fig. 4.11(d)). It should be noted that the boundary for the clustering state is ambiguous as mentioned above. Note that the macroscopic equation derived by the assumption of the unimodality of the phase distribution is irrelevant in the clustering regime. However, the unimodality recovers (at least) near the retrieval-nonretrieval critical line $\alpha_c(\beta)$. Hence, the critical line obtained theoretically according to the macroscopic description is relevant in comparing with the critical line obtained numerically.

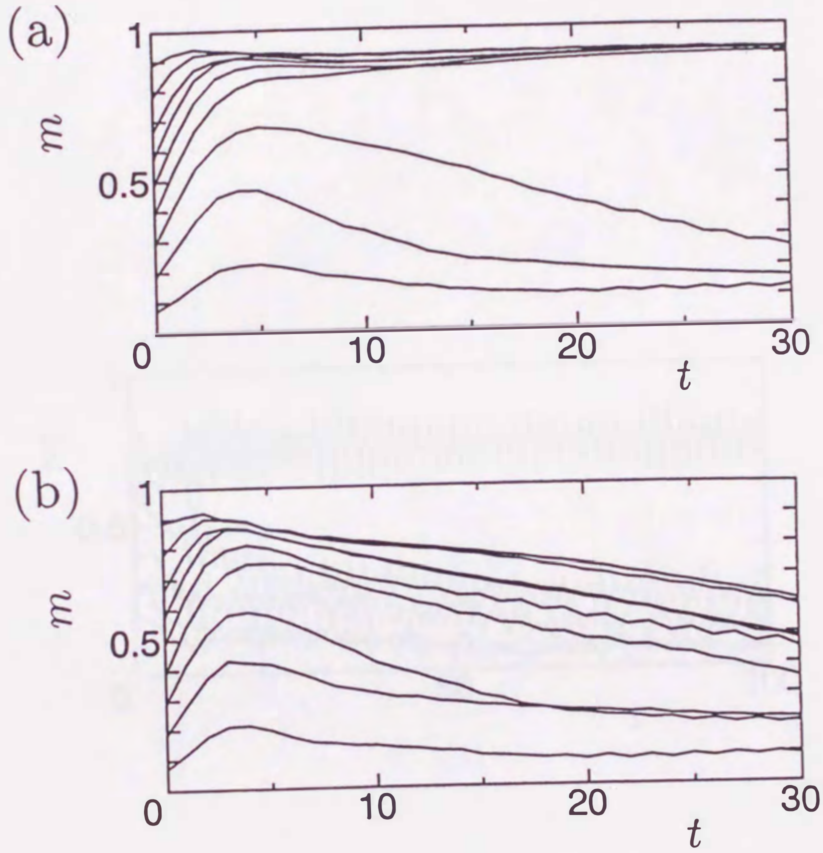

Fig. 4.8: Retrival procceses obtained numerically with $N = 700$. (a) $\alpha = 0.06$, $\beta = 1.5$, (b) $\alpha = 0.09$, $\beta = 1.5$.

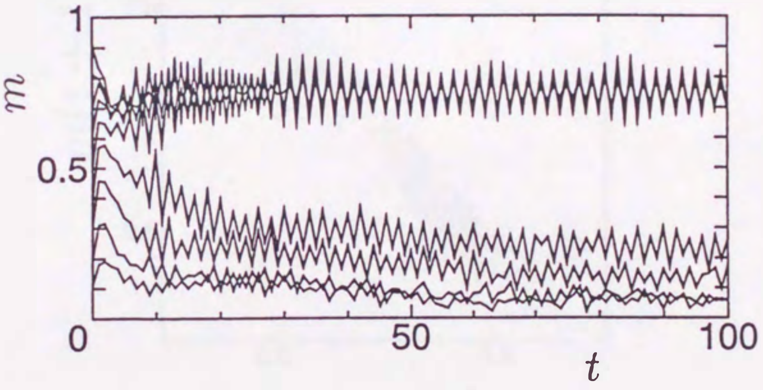

Fig. 4.9: Oscillatory retrieval processes. $\alpha = 0.1$, $\beta = 2.5$, $N = 700$.

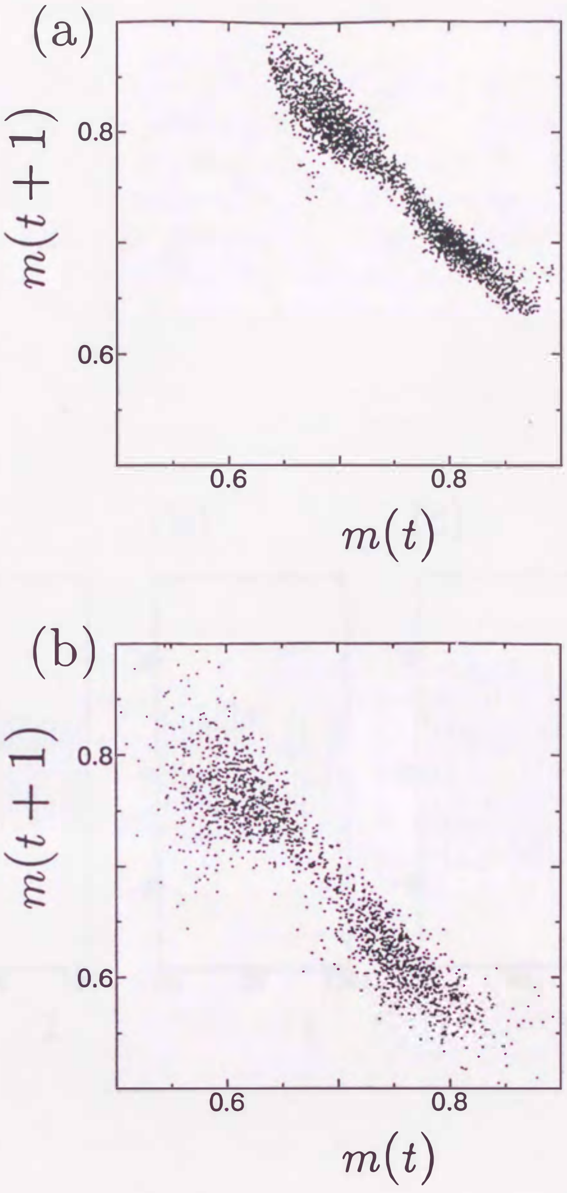

Fig. 4.10: Return map of $m(t)$. (a) $\alpha = 0.1$, $\beta = 2.5$, $m(0) = 0.9$, $N = 700$, $t = 100$–2000. (b) $\alpha = 0.1$, $\beta = 3.0$, $m(0) = 0.9$, $N = 700$, $t = 100$–2000.

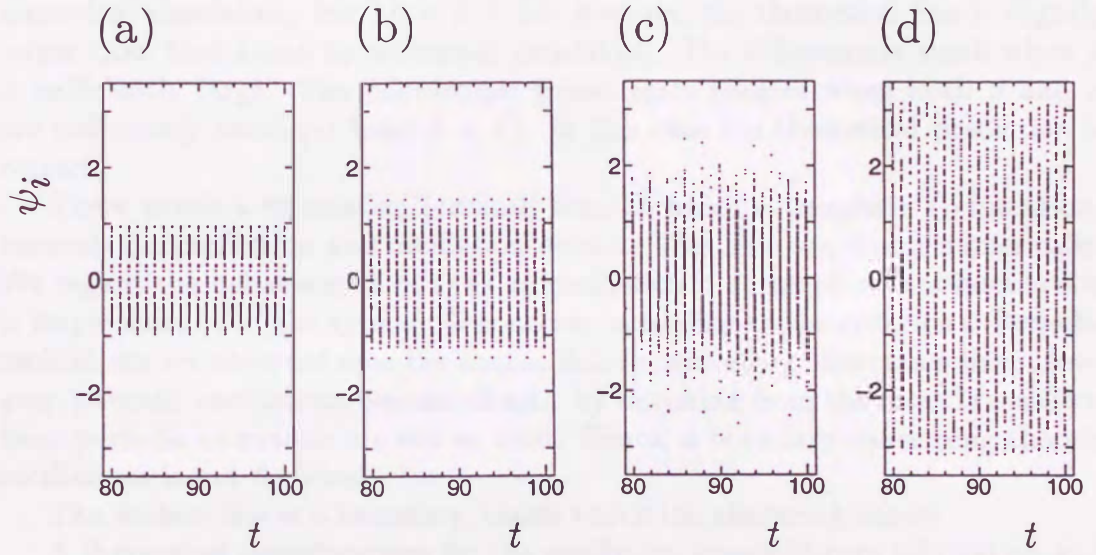

Fig. 4.11: Time evolutions of phase distribution in relatively strong nonlinear regime: β = 2.5. Phases of randomly chosen 100 oscillators from N (=700) oscillators are plotted during t = 80–100. (a) α=0.02, (b) α=0.06, (c) α=0.10, (d) α=0.20.

4.2.6 State diagram

Figure 4.12 shows the state diagram (phase diagram) with respect to the amplification factor β and the storage ratio α. Symbols dotted in this figure are corresponding to the points investigated in the numerical simulations.

In this study, the behaviour of $m(t)$ is classified into three kinds: nonoscillatory retrieval state, oscillatory retrieval state and nonretrieval state. The nonoscillatory retrieval state is observed in the weak nonlinear regime, and the oscillatory retrieval state is observed in the strong nonlinear regime, as found in Fig. 4.12.

The theoretically obtained critical line $\alpha_c(\beta)$ is also drawn. It can be found numerically that the storage capacity α_c is considerably enhanced by increasing the parameter β. However, α_c decreases when β is larger than about 3.0. We can see a fairly good agreement between the theoretical line and that found by numerical simulation. For $1.0 < \beta < 3.0$, however, the theoretical line is slightly larger than that found by numerical simulation. The difference is small when β is sufficiently large. The microscopic frozen state realizes when both β and α are sufficiently small (at least $\beta < 1$). In this case the theoretical prediction is correct.

There exists a bifurcation (critical) line, at which a transition (bifurcation) between nonoscillation and oscillation occurs. This line was found numerically. We regard the behaviour of $m(t)$ as an oscillation if an amplitude of fluctuation is larger than 0.02 (the symbol ◎ is chosen according to the criterion). Periodic oscillations are observed near the nonoscillatory-oscillatory bifurcation line. However, periodic oscillations become chaotic by deviating from the line. Transitions from periodic to chaotic are not so clear. Hence, a boundary concerning chaotic oscillations is not depicted.

The dashed line is a boundary, inside which the clustering occurs.

A theoretical considerations for the oscillatory-nonoscillatory bifurcation and the clustering are left as a future task.

4.2.7 Information content

This section is concerned with the information content (also called the information capacity), which is the amount of information embedded into the system (coupling parameters) concerned.

The storage ratio α, which is a number p of the memorized patterns normalized by the system size of N, reflects the amount of information. However, the similarity between the memorized pattern to be retrieved and the retrieved pattern should also be taken into account for estimating the amount of information carried by coupling parameters of the system concerned.

The information content in the spin-glass network model (Hopfield model) was already obtained analytically including the general case of that the memorized patterns are correlated.[96] Moreover, in what is called the Q-state clock model, the information content was also derived in the case of $Q = 2, 3, 4$ and $Q \to \infty$

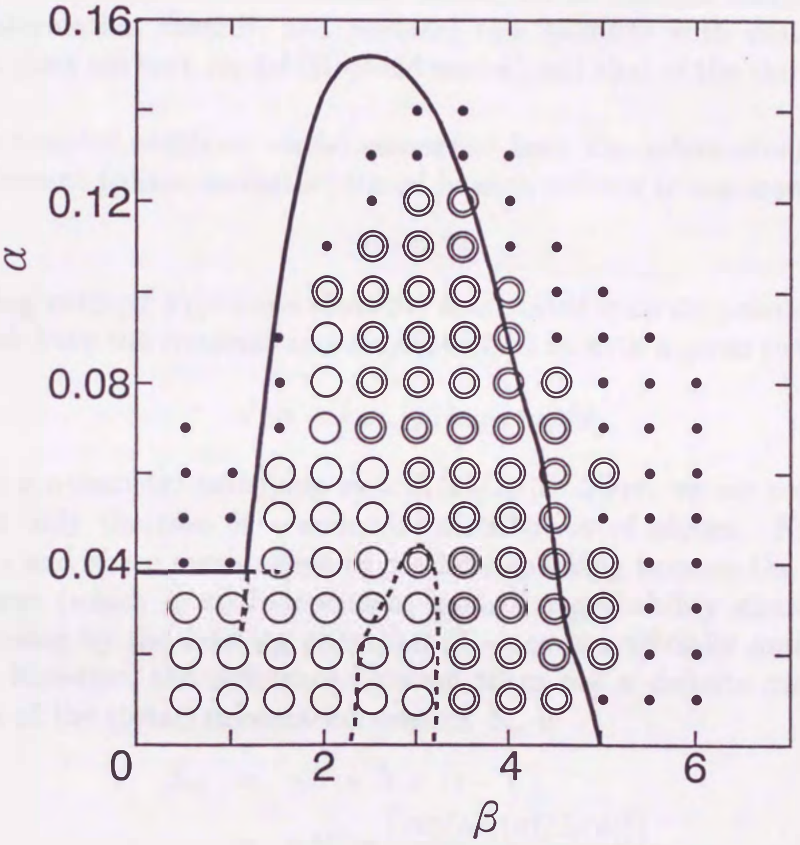

Fig. 4.12: State diagram. Numerically investigated (N = 700, m(0) = 0.9) points are indicated by symbols ○, ◎ and •, which specify nonoscillatory retrieval, oscillatory retrieval and nonretrieval, respectively. A dashed line is the boundary inside which the clustering state (2-cluster) is observed. A solid line is the retrieval-nonretrieval critical line obtained theoretically.

by Cook.[85)]

The Q-state clock model is a generalization for the two-state spin-glass model. The number Q of states of an element is assigned on a circle with equal intervals. The interaction between elementes is similar to that in the model concerned in this chapter when positions on a circle are regarded as phases. Actually, in the case of $Q \to \infty$, the behavior of the Q-state clock model is the same as that of the randomly coupled-oscillator model treated here in a simple stationary condition (or the same as that of the $X - Y$ spin glass model[97)]). Cook showed that the information content becomes infinity when Q is infinity. However his derivation was wrong in the case of $Q \to \infty$. The information content is indeed finite in spite of that Q is infinity, as will be shown. Hence, let us derive a correct expression for the information content, and compare this quantity with that of the two-state spin-glass network model (Hopfield model) and that of the three-state clock model.

In the coupled-oscillator model concerned here, the information (entropy) s per one element (phase-oscillator) stored in each pattern is expressed as

$$s = \ln 2\pi. \tag{4.36}$$

The missing entropy s'(per one element) associtated with all possible configurations which have the retrieval accuracy (overlap) m with a given pattern is

$$s' = -\int \rho_m(\phi) \ln \rho_m(\phi) d\phi, \tag{4.37}$$

where a is a parameter satisfying $m = I_1(a)/I_0(a)$. Here, we are concerning the entropy in only the case of a unimodal distribution of phases. Note that the entropies s and s' are meaningless in precisely speaking because the meaningless infinite term (which is an independent part of a probability distribution concerned) arising by the limiting operation $Q \to \infty$ is artificially omitted in each quantity. However, the difference between them has a definite meaning. The expression of the (total) information content S_∞ is

$$\begin{aligned} S_\infty &= \alpha N \times N \times (s - s') \\ &= \alpha N^2 \ln \left[\frac{\exp[a I_1(a)/I_0(a)]}{I_0(a)} \right]. \end{aligned} \tag{4.38}$$

A parameter a is a function of m, and m is a function of α and β. Hence, the information content can be specified by specifying the storage ratio α and the coupling nonlinearity β.

While, the information content S_2 of the two-state spin-glass network model is expressed as[96)]

$$S_2 = \alpha N^2 \left\{ \frac{m}{2} \ln \left(\frac{1+m}{1-m} \right) + \frac{1}{2} \ln[(1-m)(1+m)] \right\}. \tag{4.39}$$

The expression for S_3 is as[85)]

$$S_3 = \alpha N^2 \left\{ \frac{2m}{3} \ln \left(\frac{1+2m}{1-m} \right) + \frac{1}{3} \ln[(1-m)^2(1+2m)] \right\}. \tag{4.40}$$

(Note that the expression in the Cook's paper[85] is wrong. Hence, let us give a correct one.)

Here, let us show an example of a rough estimation of the information content of the coupled-oscillator system concerned here. By substituting the values: $\alpha = 0.12$, $m = 0.7$ (these values are possible when $\beta \simeq 3.0$ as confirmed by numerical simulations) into eq. (4.38), we obtain $S_\infty = 0.0691N^2$. It is found that $S_\infty = 0.0453N^2$ when $\alpha = 0.038$[85] and $\beta \ll 1$ ($m = 0.899$). Hence, it can be said that the coupling nonlinearity β brings the increase of both the storage capacity and the information content near the critical line. In the two-state spin-glass model, it is found that $S_2 = 0.0843N^2$ when $\alpha = 0.138$ ($m = 0.968$)[76]. In the three-state clock model, it is found that $S_3 = 0.222N^2$ when $\alpha = 0.22$ ($m = 0.978$)[85].

The information content of the present coupled-oscillator system even in the strong nonlinear regime is smaller than that of the two-state spin-glass network model and much smaller than that of the three-state clock model. The intuitive explanation for the origin of the superiority of the three-state clock model to others is not clear at present. Cook only showed the result obtained by the technique what is called the replica method.[85] In order to find the method to enhance the information content in the coupled-oscillator system studied here, it must be necessary to clarify the essential reason for the superiority of the three-state system, or the reason for the inferiority of the coupled-oscillator system, although it is left as a future task.

Let us mention about a possibility of increasing an effective accuracy (in effect, increasing the information content) by a certain estimation method. By the numerical simulations, it is found that there exist chaotic retrieval processes in which $m(t)$ oscillates chaotically implying a phase configuration is dynamically changing. It can be expected that the orbit in the phase-space moves around the embedded pattern to be retrieved. Hence, a certain averaging operation for the configuration of phases over a certain time interval could enhance the value of $m(t)$, although the operation is relatively artificial.

Furthermore, let us mention about an another possibility for enhancement of the information content. It should be noted that there exists another type of the embedding method what is called the sparsely encoding,[98,99] in which the patterns to be memorized are randomly generated under the constraint so that the number of firing neurons is very low compared to the total number of neurons. Theoretical consideration done by Amari[98] in the system composed of the model neurons, which take the value of an output as '0' (non-firing) or '1' (firing). The ratio of the number of firing neurons (emitting '1') to the total number of neurons N is set as $cN^{-\epsilon}$, where $c > 0$ and $0 < \epsilon < 1$. The study clarified that the information content increased by increasing the degree of the sparsity ϵ, and that the value of the information content is considerably larger than that of a non-sparse model.

It can be expected that the information content in the coupled-oscillator system concerned in the present study will be increased by the sparsely encoding method which is adequately modified to 'the coupled-oscillator version.' It should be noted that the sparsely encoding for the phase patterns means that many of the phases constituting a phase pattern will be roughly aligned with each other because the constraint for the low firing rate in the above model is corresponding to the low degrees of freedom for the configuration of phases which constitute a phase pattern to be memorized. This phase configuration means that the oscillation of the elementary oscillators is relatively coherent for observers. The coherency can be the one of the possible explanations why macroscopic (coherent) oscillations of neurons are so often observed in biological neural systems.

4.2.8 Chaotic itinerancy

In different kinds of strongly nonlinear many-body systems, the dynamical behavior what is called the chaotic itinerancy is observed.

In a certain neural network model, the chaotic itinerancy was found and studied by Tsuda.[100-102] It was found in a system of circle maps coupled globally with equal strength[63] and in other type of globally coupled-map system.[91] The phenomenon was also found experimentally in a certain optical feedback system[103] and in a nonlinear ring resonator.[104]

The chaotic itinerancy is the complex dynamics consists of quasistationary high-dimensional chaotic motion, low-dimensional attractor ruins, and switching among them.[63] In other words, the system in the state of the chaotic itinerancy choses one of the quasi-stable low-dimensional, i.e., macroscopic ordered states, and transit from one to another: the sequence of this transition seems to be chaotic.

In the language of the neural network model of associative memory, it can be said that the chaotic itinerancy is composed of non-retrieval state, incomplete retrieval of one of the memorized patterns, and apparently stochastic transition to another one. The associative memory system in the state of the chaotic itinerancy searches (retrieves) the embedded patterns one after another randomly (chaotically).

It was shown in a certain neural model[101] that there exists the network of heteroclinic orbits which play an important role for generating the phenomenon, although the detailed dynamical structure is not so clear at present. It could be true that the heteroclinic network plays an important role on other different kinds of physical systems. In the neural network model of associative memory and also in the system of coupled circle maps concerned here, there exists a saddle point near a stable equilibrium point corresponding to a memorized pattern as shown in Fig. 4.6 (b) when α is smaller than the critical value α_c. It should be noted that we can regard the unstable equilibrium point as a saddle point in the $m-\sigma^2$ space, which is a low-dimensional projection from the high-dimensional phase space. The orbital structure near the unstable equilibrium point in the high-dimensional phase space is considerably complex as in the case of a conventionl neural network model of associative memory.[61]

In the system of coupled circle maps treated here, the orbital structure between equilibrium points in the high-dimensional phase space is not clarified in the strong nonlinear regime. However, it can be expected that the strong (coupling) nonlinearity will produce a certain kind of connections between unstable or stable equilibrium points in the phase space. The complex behavior looks like the chaotic itinerancy can be observed in the model concerned here by numerical simulations. Figure 4.13 shows an example of the complex behavior in the relatively strong nonlinear regime. Considerably large fluctuation in each overlap is observed.

In this study, the dynamical behavior of this kind is classified as a non-retrieval state. However, in a wide sense, it can be considered that a certain kind of retrieval state arises. It can be found that the memorized patterns are retrieved incompletely and temporarily. The phase configuration is similar to one of the memorized patterns temporarily: the absolute value of overlap $|m^{\mu}(t)|$ (μ is an arbitrary number specifying one of the memorized patterns) is close to unity temporarily, and the value of $|m^{\mu}(t)|$ decreases. After that another one $|m^{\mu'}(t)|$ increases (μ' is another or the same number to specify the pattern to be retrieved). The selection of the memorized patterns occurs apparently stochastically. This apparent stochastic selection could be due to the structure of the heteroclinic network connecting the equilibrium points corresponding to the memorized patterns. It should be noted that in the retrieval period of one of the memorized patterns, the overlap exhibits chaotic oscillation keeping its average value close to unity. Hence, the dynamical structures near the equilibrium points are considerably complex in the model treated here.

The region in which the chaotic itinerancy occurs is not specified yet at present. The systematic investigation to specify the region and to clarify the dynamical structure should be done in the next detailed study in the future.

4.3 Discussion

In section 4.1, it is shown that the storage capacity decreases by the increase of the width of distribution of the natural frequencies, which also leads to an oscillation of the overlap $m^1(t)$. We treated the continuous-time model only in this section 4.1. No highly nonlinear phenomenon such as chaos arises, although there exist various kinds of chaotic phenomena in biological systems. Hence, the discrete-time model, in which the chaos could be reproduced, was investigated in the next section 4.2. The discrete-time model, which is also called a map system, is expected to be one of the mathematically simplest models aiming at reproducing strongly nonlinear or complex oscillatory phenomena. The model treated here is aiming at developing an associative momory system, in which phase patterns of oscillatory elements are memorized and retrieved. The introduced nonlinearity factor β is an important parameter which makes the system biffurcate from a simple state to complex states. Note that the continuous-time model can be regarded as the limitting case of $\beta \to 0$ in the discrete-time model.

In section 4.2, it has been shown that the retrieval processes in the system of randomly coupled circle maps can be fairly well described in terms of the macroscopic dynamics. The retrieval–nonretrieval critical line has also been obtained

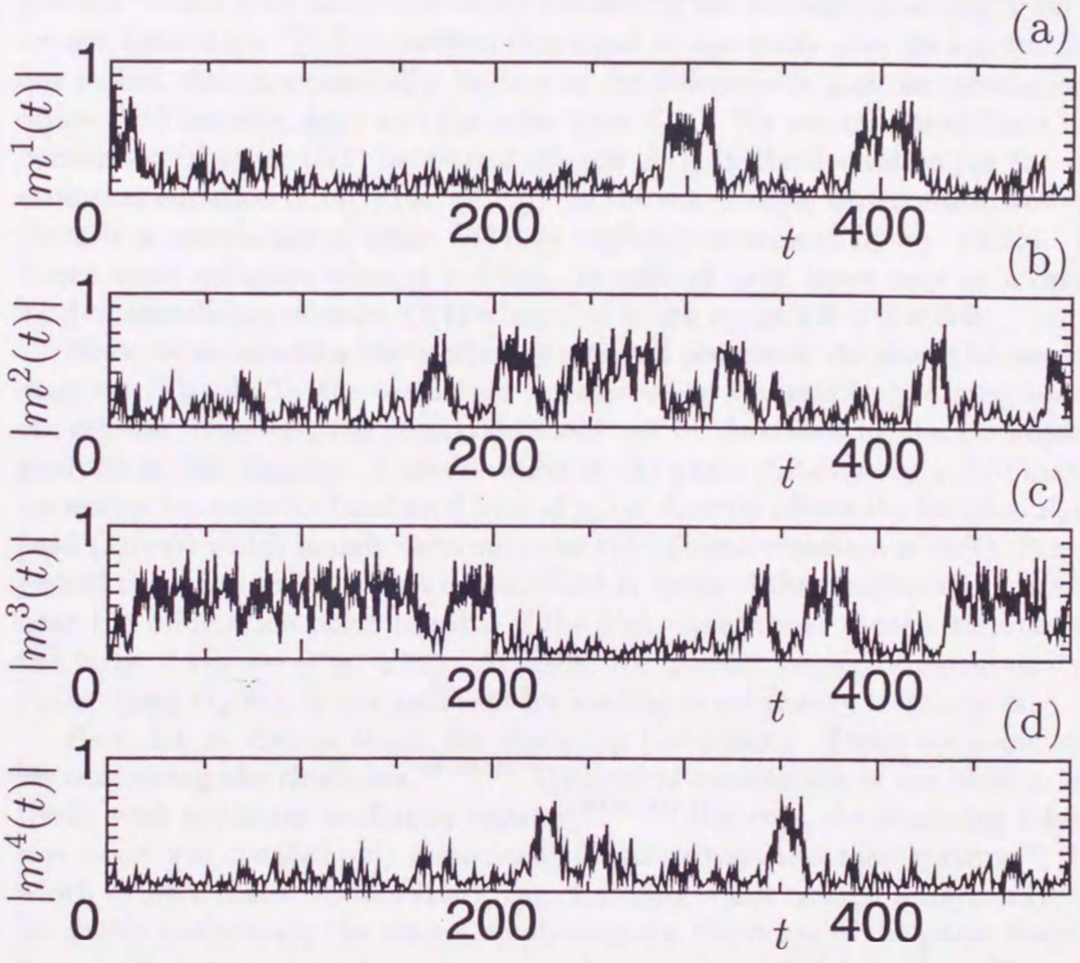

Fig. 4.13: An example of the chaotic itinerancy found in numerical simulations. $N = 500$, $\alpha = 0.008$, $\beta = 5.0$ and $m^1(0) = 0.7$. Figures (a), (b), (c) and (d) depict the dynamics of (absolute values of) overlaps $|m^1(t)|$, $|m^2(t)|$, $|m^3(t)|$ and $|m^4(t)|$, respectively.

by the macroscopic analysis. It has been shown that the theoretically obtained critical line is approximately coincident with that obtained numerically. However, the theoretical one is slightly larger than the numerical one when $1.0 < \beta < 3.0$. In the statistical calculation for $\sigma^2(t+1)$ (see Appendix C·4), we have taken the correlation at time t into account, and correlations before time t have been neglected, although the contribution of the previous correlations before the time t are implicitly taken into account by a time updating process. Hence, it is conjectured that the degree of the contribution from the former times is large when $1.0 < \beta < 3.0$, although the detailed effect of β on the correlation is not clear at present. There is an analytical study concerning the correlation arising from the former time steps.[105] The method developed in the study may be applicable to our model. Another possibility leading to the difference is that the correlation of order $O(1)$ between $\phi_i(t)$ and the noise term $Z_i(t)$. We assumed that there is no correlation of order $O(1)$ between $\phi_i(t)$ and $Z_i(t)$ in the derivation for the time evolution equation of $m(t)$ (eq. (4.22)). In the microscopic frozen state, however, there is a correlation of order $O(1)$, as explicitly expressed by eq. (4.35). The frozen state collapses when $\alpha > 0.038$. In spite of that, there may be a certain kind of correlation of order $O(1)$ when β is in the range $1.0 < \beta < 3.0$.

Next, let us consider the oscillatory retrieval processes. As shown in the state diagram (Fig. 4.12), the oscillation is observed in the relatively strong nonlinear regime. However, the oscillation could not be described by the macroscopic analysis in this chapter. A modification of the phase distribution $\rho_m(\phi)$ may be necessary, because the functional form of $\rho_m(\phi)$ directly affects the function $F_\beta(m)$ (and $G_\beta(m)$) which mainly determins the rule of time evolution of $m(t)$. It is expected that the oscillation can be described in terms of the macroscopic dynamics near the bifurcation point in spite of the high-dimensional chaotic attractors in the large β regime (Fig. 4.10). Actually, the present degree of nonlinearity of $F_\beta(m)$ (and $G_\beta(m)$) is not sufficient for leading to oscillatory instabilities.

Here, let us discuss about the clustering phenomena. There are some studies concerning the clustering.[59,90-95] Theoretical considerations are done in relatively weak nonlinear oscillatory systems.[59,93,94] However, the clustering bifurcation point was clarified only numerically in strong nonlinear map systems,[90,91,95] which exhibit chaos. In this study, the clustering is not treated analytically, too. To clarify analytically the clustering phenomena, the shape of the phase distribution $\rho_m(\phi)$ have to be extended so as to have a bimodal distribution. Moreover, a certain macroscopic variable must be introduced for reflecting the clustering. For example,

$$\begin{aligned} m_n(t) &= E[\exp[\mathrm{i}n\phi_i(t)]] \\ &= \int_{-\pi}^{\pi} \mathrm{e}^{\mathrm{i}n\phi}\rho_m(\phi)\mathrm{d}\phi, \quad n = 1, 2, \cdots \end{aligned} \tag{4.41}$$

may be relevant. The macroscopic variable $m_n(t)$ can be regarded as the n-th Fourier component of $\rho_m(\phi)$, where m represents a set of variables $m_1(t)$, $m_2(t)$,$\cdots$, which could carry a large amount of information about the phase distribution. Then, a set of equations of $m_n(t)$, $n = 1, 2, \cdots$, is necessary.

Next, let us comment on the effect of the natural frequency distribution on the macrodynamics, which can be taken into account theoretically (see Appendix C·5). The distribution works as an external noise, which causes the decrease of the storage capacity α_c, as in the time-continuous system of randomly coupled phase oscillators.[86)]

Here, we would like to discuss about an external force on the system. The external force can be expected to work as the support (or disturbance) for retrieval, or other certain functions unexpected. One of our main interests is to clarify the dependences of both the retrieving speed and the accuracy of the retrieval on the storage ratio α and the coupling nonlinearity β when the system is under the external force, especially in the strongly nonlinear regime. The modified model into which the external force is taken account is expressed as

$$\begin{aligned}\phi_i(t+1) &= \phi_i(t) + \omega_i + \beta \sum_{j=1}^{N} K_{ij} \sin(\phi_j(t) - \phi_i(t) + \varphi_{ij}) \\ &\quad + J \sin(\tilde{\theta}_i - \phi_i(t)), \quad i = 1, \cdots, N, \end{aligned} \tag{4.42}$$

where the last term represents the external force, in which a parameter J means the strength of the external force, and $\tilde{\theta}_i$ is the i-th component of the input phase pattern. The input pattern $\{\tilde{\theta}_i\}$ may be specified so as to be similar to one of the embedded patterns. The similarity $\widetilde{m}$ between the input pattern $\{\tilde{\theta}_i\}$ and e.g., $\{\theta_i^1\}$ will be expressed as

$$\widetilde{m} = \frac{1}{N} \sum_{i=1}^{N} \exp[\mathrm{i}(\tilde{\theta}_i - \theta_i^1)]. \tag{4.43}$$

What we have to do is to investigate the dependence of the retrieving speed and retrieval accuracy on $\widetilde{m}$, α, β and J. The external force is expected to be sufficiently small ($J \ll 1$) so as not to change considerably the original behavior without it. However, when the external force is specified so that it can be regarded as the 'support input' for promoting retrieving processes (it means that $\widetilde{m}$ is sufficiently close to 1), the input can be expected to bring wider regime of the retrieval state especially in the case of the chaotic itinerancy. This is because the state of chaotic itinerancy in the system might be regarded as a certain kind of critical state, in which the system will obey easily the external input, as in the case of a ferromagnetic system which is very sensitive to the external magnetic field, although the essential dynamics in the system treated here is different from that in ferromagnetic systems.

Lastly, let us comment on the possibility that the chaos enhances the speed of information processings in the present coupled-oscillator systems as an associative memory machine. A retrieving process can be regarded as a synchronization process in which the system state goes towards the specified phase-configuration to be retreived. It is obvious that the speed of retrieving should be sufficiently high, from the view point of engineering. (The characteristic time τ_{R} of the retrieving can be expected to be roughly proportional to the inverse of the coupling strength: $\tau_{\mathrm{R}} \sim (|\beta K_{ij}|)^{-1}$, although the systematic and detailed investigation is left as a future task.) Here, note that also the desynchronization speed should be high enough. The rapid desynchronization (dephasing) is necessary to do the rapid information process for the sequence composed of many phase patterns (, which might be input into the system in practical use,) because the dephasing must be done before the next retrieving of a phase pattern, which is one of the components constituting the sequence concerned. The chaos is one of the candidates for promoting the dephasing and destroying a phase pattern. When the system is in the chaotic state the characteristic time τ_D of the dephasing must be corresponding to that of the separation of neighboring orbits of the systems in an ensemble concerend in the phase space. If the separation can be measured by the Liapunov exponent λ, it can be naturaly said that $\tau_D \sim \lambda^{-1}$. Therefore, larger the degree of chaos (measured by λ), smaller the dephasing time τ_D or more rapid destroying the retrieved phase pattern. (The rapid desynchronization by chaos has already been discussed by Hansel et al.[54]) Whereas, another candidate is the noise, which will be applied to the elementary oscillators without any spatial correlations. The noise will lead dephasing, but it will take very long time to desynchronize because the separation of the orbits does not obey an exponential manner ($\sim \exp(\lambda t)$) but a manner of power ($\sim t^{\xi}$, $\xi > 0$) with respect to time.

5 Conclusions

Nonlinear dynamics as neural activities in a certain type of coupled-oscillator systems have been studied. In the system studied here, a state of an each of the elementary oscillators is specified only by the phase. Each oscillator is affected by forces depending only on relative differences of phases between the one concerned and the others'. By investigating the dynamic behaviors of these simple systems, we have shown the followings.

1: The present coupled-oscillator system of the 'natural-frequency variable type' can have capabilities for learning and recognition of some kinds of periodic temporal signals by introducing the learning rule which changes adaptively the distribution of natural frequencies of the elementary oscillators.

2: The above system exhibits a bifurcation from a simple ordered (or disordered) macroscopic state to complex (chaotic) oscillatory states by varying parameters of the input signals.

3: The system can be considered to have capabilities for recognizing degrees of difference between the learned pattern and the input pattern through the degree of complexity of the output oscillatory behavior. Transient oscillatory behaviors depending on paramaters of the input signals are also found. This transient behavior can be regarded as another way of representation for the difference between the learned one and the input.

4: The coupled-oscillatory system of the 'coupling-strength variable type' can learn a desirable mapping from a stationary phase pattern to output an analog value. The main feature of the system is to have the analog output of phase-coherency of oscillators of the output unit. The capability is realized by introducing the (modified) Boltzmann-machine learning rule which changes coupling strengths between oscillators.

5: It is found that the interpolation characteristic is self-organized in the learning process. The characteristic means that the system can adequately respond to the input of unlearned pattern by emitting an adequate value of output. The output value is affected by the already-learned correspondings between input patterns to output values.

6: It is found that the interpolation charecteristics are partially destroyed by introducing the distribution of natural frequencies of the elementary oscillators. In the destroyed regime, the system exhibits the macroscopic chaotic behavior, which may indicate that the system gives up the recognition of the input pattern because of too long distance between the input pattern and the learned pattern. It should be pointed out from the view point of engineering that the chaotic behavior may be available as the 'trigger' to start to learn the unlearned pattern.

7: The coupled-oscilltor system of the 'associative memory machine' exhibits behaviors which are fundamentally similar to those of conventional neural-network models. The distribution of natural frequencies works as an external noise, such as thermal fluctuation.

8: In the above system, macroscipic chaotic behaviors are found by increasing the coupling nonlinearity. The clustering phenomenon of phase distribution is also found in a certain strong nonlinear regime. The nonlinearity also enhances the storage capacity considerably. The statistical mechanical analysis can provide a set of macroscopic dynamical equations which can describe retrieving processes and explain the enhancement of the storage capacity, although the chaotic behavior has not been analytically described. It is found that the maximum values of storage capacity and information content (capacity) are relatively smaller than those of the spin-glass neural network model. Therefore, it is necessary to find the way to improve the capacities.

9: The dynamic behavior called the chaotic itinerancy is found when the coupling amplification factor is sufficiently large. One of the memorized patterns are randomly selected and retrieved incompletely, chaotically and temporally. After that the selected pattern is forgotten and one of the other patterns is again randomly selected to be.

At the present paper, we have tried to clarify possibilities and limitations of the systems composed of phase-oscillators for modeling brain functions and for engineering applications such as constructing a pattern recognition system. We have tried to characterize the high-dimensional oscillatory system by investigating nonlinear responses to various input patterns, learning processes, storage capacity, retrieval processes, information content, and strong nonlinear complex (chaotic) dynamics.

The effect of coupling nonlinearity and distribution of natural frequencies on the (macroscopic) oscillatory dynamics is one of the main subjects on which we focus our attention in the present study. It can be considered that the distribution of natural frequencies (together with a coupling effect) induces the complex (chaotic) oscillatory responses as a function for measuring similarity between an input pattern and one of learned patterns. The complex oscillatory responses can also be considered as a trigger signal for activating certain learning proceses which are expected to be existing in real biological nervous systems.[14)]

Although the storage capacity and information content in the coupled-oscillator models treated here is relatively less than those of conventional spin-glass type neural network models, there exist certain kinds of nonlinear dynamics, which have not been found in conventional neuro models. One of the nonlinear dynamics such as complex oscillatory response can be expected to be effective for a system to incorporate self-decision ability to start learning. The chaotic response function to unlearned inputs could be considered as the "New-Pass-Filter."[15)] The chaotic retrieval dynamics in the coupled-oscillator system as an associative memory machine concerned here will be used for generator for random patterns which have the same similarities (distances) to a certain target pattern in a phase space defined by an adequate metric.

The strong coupling nonlinearity is implying strong distortion of a high-dimensional torus corresponding to the dynamical structure of the system concerned. It is found that the distortion brings not only the enhancement of the memory capacity but the nonlinear dynamics called the chaotic itinerancy.

The chaotic itinerancy could be utilized for memory search, although there is no analytically clear evidence of superiority to a conventional random search.

There exist some studies concerning chaotic search in a certain neuro models.[101,106] Furthermore, the chaotic itinerancy can be regarded as a process of the self-organized generation of a rule which establishes certain connections between memorized patterns.[101]

The future tasks are the followings.

(1) To find the way for improving the storage capacity and information content. The sparse coding may be relevant for this purpose.

(2) To clarify the underlying mechanisms of nonlinear dynamics such as the chaotic retrieval, clustering and chaotic itinerancy.

(3) To find the way for engineering application of the above strong nonlinear dynamics by showing superiorities of the oscillatory information processings to conventional spin-glass type information processings or to digital processings.

(4) To establish the way for implemantation of the nonlinear dynamics obtained here to electric circuits (such as a system of PLL networks) or other types of physical or chemical systems (such as a system of coupled Josephson junction networks). It is aiming at constructing a certain new type of computer dealing with oscillatory information processings.

(5) To show the way of electrophysiological experiments in animal brains for making possible to compare explicitly between the results obtained in this study and information dynamics executed in biological neural systems. It is aiming at clarifying the underlying mechanisms of the oscillatory information processings observed in animal nervous systems.

Next, let us mention about some directions for developing this study. There are some interesting remaining subjects.

One is to investigate dynamics in the case of asymmetric couplings. The assumption of symmetric coupling makes the statistical analysis easier. However, this assumption is quite artificial, and could not hold in real biological nervous systems. At first, we may try a perturbation technique in which a small asymmetric coupling factor is taken into account as a perturbation. The assumption that an asymmetric factor is small may be still artificial. So, it may be necessary to develop a certain new method to deal with a large asymmetric factor.

Another is to investigate effects of noise on the copuled-oscillator system. The effect of noise on nonlinear systems is not so simple in general cases. For example, the effect of multiplicative noise can change bifurcation structures.[107] There is a phenomenon called stochastic resonance on which many researchers are paying their attentions. The stochastic resonance is a phenomenon wherein the response of a nonlinear system to a certain weak input signal is optimized by the presence of a particular level of noise. There are a lot of papers on concerning this subject in various kinds of physical systems including systems composed of many coupled elements[108-111] and neural models.[112-114] However, there is no study concerning stochastic resonance in a strong nonlinear coupling system exhibiting high-dimensional chaos.

And, another is to investigate dynamics in the system under the chaos control. The technique of controlling chaos is the method for stabilizing unstable chaotic orbits.[115] The technique and some modifications are applied various kinds of physical systems including biological neural systems.[11] There exist some studies on controlling chaos for systems composed of coupled elements or spatially extended systems.[55,116-119] However, there is no study concerning the chaos control in a system composed of strongly coupled circle maps.

Acknowledgements

The present paper is composed of the results obtained in the studies during 1993–1996.

I would like to express cordial thanks to Prof. Kaoru Yamafuji and Prof. Kiyoshi Toko for their kind encouragements for the present study. Their useful comments and suggestions helped me to develop the present work and to complete the present paper.

I would also like to express much thanks to diligent graduate school students Ms. Yukiko Kikkawa and Mr. Masahiro Iguchi (They are now working in companies.). They directly supported the present work by numerical simulations and valuable discussions. I often obtained useful ideas in discussions with them.

Moreover, I am very grateful to Prof. Tetsuo Nishi and Prof. Tohru Kohda for their valuable comments and suggestions which helped me to make several improvements of the manuscript.

And, I want to say thank you to other sutudents and staffs in the Yamafuji-Toko lab. for their encouragements and various kinds of helps such as constructing comfortable computer environment and making some tea and coffee.

Appendices

A Supplement for Introduction

A·1 Physiological Background

There exist various kinds of oscillatory phenomena in biological neural systems. Nonlinear oscillatory phenomena such as synchronization and chaos are often observed over wide range from a single neuron to a network of neurons. Chaotic behaviors are observed in the *Onchidium* neuron,[5,6] the giant axon of a squid,[7,8] the transverse hippocampal slice of a rat,[9-11] the visual cortex of a cat,[12,13] the olfactory bulb of a rabbit[14,15] and the electroencephalogram from the human brain.[16]

Various kinds of informations are considered to be carried by sequences of electrochemical impulses generated by neurons and transmitted by axons. In order to clarify underlying mechanisms of brain functions, many researchers have been investigating densities of pulses in sequences to obtain functional correlations among a group of neurons under consideration. The problem which may arise in the above conventional method is that there exists a possibility to miss a certain amount of important information by an average operation over a certain temporal interval. The interval for averaging may be much larger than a certain characteristic time-scale of the underlying chaos dynamics which may be playing an important role for information processings carried by the sequence of the impulses. However, by introducing an adequate technique to reconstruct an orbit corresponding to the dynamics concerned, chaotic behavior (implying it is a deterministic chaos) can be observed and can be characterized quantitatively in some cases, which are the examples refered in the above.

Let us explain simply some of the electrophysiological studies concerning nonlinear oscillatory dynamics. Synchronization phenomena in the visual cortex of a cat was found by Gray and Singer[12,13] relatively recently. They found that the neuronal firing pattern oscillated in the range of 40-60 Hz, and that the firing patterns in certain different areas are considerably correlated (synchronized) when a certain visual stimulus was given. The stimulus is the two bars moving the same direction on a screen in front of a cat. The synchronization did not occur if the moving directions are different. The above observations suggest that oscillations and synchronized oscillations play an important role for the visual information processing what is called the binding, in which the neural system determins whether a certain segment belongs a figure to which the cat pays attention.

A certain relationship between chaos and the pattern recognition processes in the olfactory system in a rabbit was found by Freeman.[14,15] in the investigation of responses of the electrical activities to different kinds of smells. It is found that regular oscillations were observed when the learned smells were given, while chaotic oscillations occured if the unlearned (unknown) smells were given. However, the chaotic response changed to a regular oscillation when a rabbit had finished learning the target smell unlearned. The above observations suggest that The chaotic response is a signal to show "unknown" and to activate a learning procedure.

A slice sample of the hippocampus, which is regarded as a system being responsible for memorizing processes and crucial actions for survival, is one of the popular materials for neuro-physiologists because it is possible to do experiment in vitro. However, the undoubted evidence of chaotic activity in the hippocampus of a rat was obtained relatively recently by Hayashi et al.[10] Nonlinear oscillatory phenomena such as phase-locking (synchronization), noise-induced strange fluctuations and chaos were observed under external periodic stimulations. The observed chaos is low-dimensional because of strong connections among neurons. Hence, the analysis for it was done relatively easily compared to that for the high-dimensional chaos which may exist in wide area of biological neural systems.

Other electrophysiological studies in neural systems also shows that there exist various kinds of nonlinear oscillations in various time scales.

It is important to investigate nonlinear oscillations in various specific models of the biological neural systems. Whereas, it is also important to construct a simple (mathematically solvable) model for aimig at extracting fundamental underlying mechanisms for oscillatory information processings. Recent technology such as the multi-channel optical recording makes possible to observe spatio-temporal neural activities in high resolution. However, at present, we do not have the method to interpret the reconstructed high-dimensional orbits from the obtained signals. Collaborations of experimental physiological studies and the studies of nonlinear dynamical structure in simple models are quite necessary for clarifying the essential mechanisms in the oscillatory information processings in neural systems.

A·2 Circle Map and Coupled Circle Maps

A circle map was introduced as the simple mathematical model for investigating universalities concerning strong nonlinear dynamics (chaos) in oscillatory systems[23-26] such as periodic forced pendulum, the Josephson junction system, charge density wave system, and so on. Universal (scaling) behaviors were clarified theoretically by using renormalization techniques,[120,121] and other techniques[122]

The circle map is expressed as

$$\phi(t+1) = \phi(t) + 2\pi\Omega - K\sin\phi(t), \tag{A.1}$$

where a certain oscillatory system under periodic perturbation is considered. The variable $\phi(t)$ is an angular component in a polar coordinate expanded in the Poincaré plain which cut the orbit corresponding to the dynamics of the oscillatory system concerned, and the variable specifies the t-th cutting position. Note that t in eq. (A.1) is not a time, but it can be considered as a discrete-time in a sense.

The state of the system is assumed to be well characterized by one variable, i.e., a phase, which is the original continuous-time variable to be discretized to the discrete-time one: $\phi(t)$. The parameter Ω is the ratio of the natural frequency of the system to that of the external perturbative force. That is $\Omega = \omega_{\mathrm{I}}/\omega_{\mathrm{O}}$, where ω_{I} is the natural (angular) frequency of the system concerned and ω_{O} is that of the external force. The parameter K represents the strength of the external force or the strength of coupling between the system and the source of the external force.

It was shown numerically[26] that the map (eq. (A.1)) can describe essential dynamics in some periodic forced systems described by a differential equation such as

$$\frac{d^2\phi}{dt^2} + C\frac{d\phi}{dt} + D\sin\phi = A + B\cos\omega_{\mathrm{O}}t, \tag{A.2}$$

where t in the above eq. (A.2) is a continuous-time, and coefficients A, B, C and D are arbitrary parameters characterizing the system. Of course, a circle map is expected to describe dynamical behaviors in other types of periodic forced systems. Indeed, it was found that some critical factors obtained by the circle map were agree with those obtained experimentally in a fluid system such as a (periodic) forced Rayleigh-Bénard system.[123] Although the systematic method for reduction from eq. (A.2) to eq. (A.1) is not known at present, study of the circle map reveals the fundamental characteristics to produce universal behaviors.[23-26,120,121] Hence, it is intuitively expected that the fundamental dynamical structure of the system composed of many oscillators coupled to each other will be clarified by investigating a mathematically simple model as the coupled-map system treated in this study.

The circle map (eq. (A.1)) describes a certain deterministic rule of updating of a phase specifying a position in a closed circular orbit (1-torus), which is the Poincaré section of a 2-torus corresponding to oscillatory dynamics (such as quasi-periodic oscillations and chaos) in periodic forced systems. Smilarly, the coupled circle maps can be expected to describe a certain deterministic rule of updating of a set of N phases specifying a position in an N-torus, which is the Poincaré section of an $(N+1)$-torus corresponding to high-dimensional oscillatory dynamics in a certain periodic forced system. The number N represents degrees of freedom of the system under (external) periodic force, and $N+1$ is a whole dimension including a freedom of motion corresponding to the external periodic force. Note that the external periodic force do not have to perturb effectively the system concerned, and in general, it will work just as a pace-maker or a clock which is detemining an interval of sampling the values of phases of the constituent oscillators.

The oscillatory dynamics in a biological neural network system or a fluid system may be described by e.g., the coupled Hodgkin-Huxley equations or the coupled Navier-Stokes equations, which are coupled differential (continuous-time) equations. It can be expected that the fundamental oscillatory characteristics in such a sytem are well described by a system of coupled circle maps. However, the systematic reduction method for obtaining correspondences between parameters in the circle map system and those in the original (continuous-time) system is not known. Hence, one of what we can do for clarifying strong nonlinear dynamics in high-dimensional oscillatory systems is to investigate intensively the dynamics in the simple mathematical model such as the coupled circle maps[63] or other types of simple coupled-map systems such as a system of coupled logistic maps[90] or a system of coupled standard maps. A what is called the standard map[124-128] contains the information on an amplitude of the oscillation in a system concerned. The system of coupled standard maps may be a good model in some cases.

B Details of Calculations in Chapter 3

B·1 Analysis of the Learning

Here, we will show the analysis for ensuring the realizability of the specified mapping: $\phi_I \longrightarrow \widehat{R}$. The explicit forms of the stationary conditional probabilities can be expressed as follows:

$$f_-(\widehat{R}|\phi_I) = \frac{\int d\phi_H \int_{S(\widehat{R})} d\phi_O \exp[-U_-(\phi)/T]}{\int d\phi_H \int d\phi_O \exp[-U_-(\phi)/T]}, \tag{B.1}$$

$$f_+(\widehat{R}|\phi_I; \widehat{R}_S) = \frac{\int d\phi_H \int_{S(\widehat{R})} d\phi_O \exp[-U_+(\phi; \widehat{R}_S)/T]}{\int d\phi_H \int d\phi_O \exp[-U_+(\phi; \widehat{R}_S)/T]}, \tag{B.2}$$

where $f_-(\widehat{R}|\phi_I)$ is the conditional probability of finding that the system exhibits $\widehat{R} = R(\phi_O)$ when the phases of the input oscillators are specified at ϕ_I in the free mode. The function $f_+(\widehat{R}|\phi_I; \widehat{R}_S)$ is the conditional probability of finding that the system exhibits $\widehat{R} = R(\phi_O)$ when the phases of the input oscillators are specified at ϕ_I and the supervisor signal is specified at $\widehat{R}_S$ in the learning mode. The integration operator $\int_{S(\widehat{R})} d\phi_O$ means the integration on the hyper-surface specified by the constraint $\widehat{R} = R(\phi_O)$ in the ϕ_O-space (the phase-space of the output oscillators).

Here, we introduce the functional,

$$F = \int d\widehat{R} \int d\phi_I \, g(\widehat{R}, \phi_I) \ln \frac{f_+(\widehat{R}|\phi_I; \widehat{R})}{f_-(\widehat{R}|\phi_I)}, \tag{B.3}$$

which was already shown in section 3.2.1. The aim in this appendix is to show that the functional F decreases monotonously by updating the connectivities K_{ij} obeying the rule adopted here expressed by eq. (3.15). We can easily obtain the following relations:

$$\begin{aligned} 2NT\frac{\partial}{\partial K_{ij}} \ln f_-(\widehat{R}|\phi_I) = \\ \frac{\int d\phi_H \int_{S(\widehat{R})} d\phi_O \cos(\phi_j - \phi_i) \exp[-U_-(\phi)/T]}{\int d\phi_H \int_{S(\widehat{R})} d\phi_O \exp[-U_-(\phi)/T]} \\ -\frac{\int d\phi_H \int d\phi_O \cos(\phi_j - \phi_i) \exp[-U_-(\phi)/T]}{\int d\phi_H \int d\phi_O \exp[-U_-(\phi)/T]}, \end{aligned} \tag{B.4}$$

$$\begin{aligned} 2NT\frac{\partial}{\partial K_{ij}} \ln f_+(\widehat{R}|\phi_I; \widehat{R}) = \\ \frac{\int d\phi_H \int_{S(\widehat{R})} d\phi_O \cos(\phi_j - \phi_i) \exp[-U_+(\phi; \widehat{R})/T]}{\int d\phi_H \int_{S(\widehat{R})} d\phi_O \exp[-U_+(\phi; \widehat{R})/T]} \\ -\frac{\int d\phi_H \int d\phi_O \cos(\phi_j - \phi_i) \exp[-U_+(\phi; \widehat{R})/T]}{\int d\phi_H \int d\phi_O \exp[-U_+(\phi; \widehat{R})/T]}. \end{aligned} \tag{B.5}$$

Here, let us note that the following relation:

$$
\begin{aligned}
& U_+(\phi;\hat{R}) - U_-(\phi) \\
&= \frac{J}{2M}\sum_{i\in O}\sum_{j\in O}\cos(\phi_j-\phi_i) \\
&\quad -J\hat{R}\sqrt{\sum_{i\in O}\sum_{j\in O}\cos(\phi_j-\phi_i)} + \frac{M}{2}J\hat{R}^2 \\
&= \frac{M}{2}J[R(\phi_O)-\hat{R}]^2. \qquad \text{(B.6)}
\end{aligned}
$$

And, by considering the fact that $R(\phi_O) = \hat{R}$ during the integration process $\int_{S(\hat{R})} d\phi_O$, it is found that the first term of the right hand side of eq. (B.4) is equal to that of eq. (B.5). Therefore, the relation:

$$
\begin{aligned}
& -2NT\frac{\partial}{\partial K_{ij}}\ln\frac{f_+(\hat{R}|\phi_I;\hat{R})}{f_-(\hat{R}|\phi_I)} = \\
& \int d\phi_H \int d\phi_O \cos(\phi_j-\phi_i)[f_+(\phi_O,\phi_H|\phi_I;\hat{R}) - f_-(\phi_O,\phi_H|\phi_I)]
\end{aligned} \qquad \text{(B.7)}
$$

is obtained.

Here, the conditional probabilities $f_+(\phi_O,\phi_H|\phi_I;\hat{R})$ and $f_-(\phi_O,\phi_H|\phi_I)$ are expressed as follows:

$$
f_-(\phi_O,\phi_H|\phi_I) = \frac{\exp[-U_-(\phi)/T]}{\int d\phi_H \int d\phi_O \exp[-U_-(\phi)/T]}, \qquad \text{(B.8)}
$$

$$
f_+(\phi_O,\phi_H|\phi_I;\hat{R}) = \frac{\exp[-U_+(\phi;\hat{R})/T]}{\int d\phi_H \int d\phi_O \exp[-U_+(\phi;\hat{R})/T]}. \qquad \text{(B.9)}
$$

From all of the above, we obtain

$$
\begin{aligned}
& -2NT\frac{\partial}{\partial K_{ij}}F \\
&= \int d\hat{R}\int d\phi\{g(\hat{R},\phi_I)\cos(\phi_j-\phi_i) \\
&\quad \times[f_+(\phi_O,\phi_H|\phi_I;\hat{R}) - f_-(\phi_O,\phi_H|\phi_I)]\} \\
&= E_+[\cos(\phi_j-\phi_i)] - E_-[\cos(\phi_j-\phi_i)]. \qquad \text{(B.10)}
\end{aligned}
$$

The above equation expresses that the functional F decreases when the connectivities K_{ij} is updated according to the rule expressed by eq. (3.15).

Next, let us consider the relation between the decrease of the functional F and learning of the specified mapping. It can be found that

$$
\begin{aligned}
& \frac{f_+(\hat{R}|\phi_I;\hat{R})}{f_-(\hat{R}|\phi_I)} = \\
& \frac{\int d\phi_H \int d\phi_O \exp[-U_-(\phi)/T]}{\int d\phi_H \int d\phi_O\{\exp[-U_-(\phi)/T]\exp[-\frac{MJ}{2T}(R(\phi_O)-\hat{R})^2]\}} \geq 1,
\end{aligned} \qquad \text{(B.11)}
$$

by noting that

$$\int_{S(\hat{R})} d\phi_O \exp[-U_+(\phi;\hat{R})/T] = \int_{S(\hat{R})} d\phi_O \exp[-U_-(\phi)/T], \tag{B.12}$$

which was already mentioned. It can be said that the last inequality in the right hand side of eq. (B.11) indicates

$$F \geq 0, \tag{B.13}$$

by considering the fact that probabilities are positive. We can say that the eqs. (B.10), (3.15) and (B.13) mean that the funcitonal F will converge to the zero value by updating the connectivities. A lot of numerical simulations showed that the functional F approached to the zero value in most cases. The approach of the F to the zero value means that the ratio $f_+(\hat{R}|\phi_I;\hat{R})/f_-(\hat{R}|\phi_I)$ approaches to the unity. We can say that the factor $\exp[-U_-(\phi)/T]$ has a sharp peak at the position: $\phi = (\hat{\phi}_I, \hat{\phi}_H, \hat{\phi}_O)$, where the symbol $\hat{\phi}_I$ represents the specified input phase pattern, and the symbols $\hat{\phi}_H$ and $\hat{\phi}_O$ represent the configuration of the phases realized when the specified pattern $\hat{\phi}_I$ is input into the system (of course, $R(\hat{\phi}_O) = \hat{R}$). The sharpness of the peak is corresponding to the closeness of the ratio $f_+(\hat{R}|\phi_I;\hat{R})/f_-(\hat{R}|\phi_I)$ to the unity, i.e., the closeness of the functional F to the zero. Moreover, as seen in eq. (B.1), the sharpness of the factor $\exp[-U_-(\phi)/T]$ is the degree of the possibility of realizing the specified output value $\hat{R}$ when the specified input $\hat{\phi}_I$ is input into the system. In the numerical simulation, the sharpness can be recognized by looking at the result shown in Fig. 3-3 in section 3.2.3.

Let us mention about the extension of the learning. We investigated about the mapping: the vector (phase pattern) to the scalar (phase coherency). The extension from the scalar output to the vector output is quite easy; i.e., we only have to introduce some groups of the oscillators as the output units. The analysis will be done without any fundamental change of the method shown here.

B·2 Definition of the Distance and the Orbit

Let us introduce a similarity between phase-pattterns $\phi_I = (\phi_i)$ and $\phi'_I = (\phi'_i)$ for $i \in I$, in input pattern-space. It seems to be natural to use the following expression as the definition of the similarity (a certain kind of an inner-product renormalized by a number of components):

$$\mu(\phi_I, \phi'_I) = \frac{1}{N_I}\sum_{i\in I}\cos(\phi_i - \phi'_i), \tag{B.14}$$

by considering that the form of the basic equation is 2π-periodic. However, the above difinition is not suitable to describe the similarity because the basic equation is invariant under the simultaneous exchange of all the variables ϕ_i for $\phi_i + c$, where c is a certain arbitrary value. That is, the system concerned here is symmetric under rotation, which means that the system cannot discriminate between a pattern $\boldsymbol{\phi} = (\phi_i)$ and a pattern, say, $\boldsymbol{\phi}_c = (\phi_i + c)$. Hence, we should reconsider the definition, and decided to define the similarity $\mu(\boldsymbol{\phi}_I, \boldsymbol{\phi}'_I)$ as

$$\mu(\boldsymbol{\phi}_I, \boldsymbol{\phi}'_I) = \max_c\{\tilde{\mu}(\boldsymbol{\phi}_I, \boldsymbol{\phi}'_I; c)\}, \tag{B.15}$$

where

$$\tilde{\mu}(\boldsymbol{\phi}_I, \boldsymbol{\phi}'_I; c) = \frac{1}{N_I}\sum_{i\in I}\cos(\phi_i - \phi'_i + c). \tag{B.16}$$

By calculating $(\partial/\partial c)\tilde{\mu}(\boldsymbol{\phi}_I, \boldsymbol{\phi}'_I; c) = 0$ for getting c, we can obtain the expression:

$$\begin{aligned} &\mu(\boldsymbol{\phi}_I, \boldsymbol{\phi}'_I) \\ &= \frac{1}{N_I}\sqrt{(\sum_{i\in I}\cos(\phi_i - \phi'_i))^2 + (\sum_{i\in I}\sin(\phi_i - \phi'_i))^2} \\ &= \frac{1}{N_I}\sqrt{\sum_{i\in I}\sum_{j\in I}\cos(\phi_i - \phi'_i - \phi_j + \phi'_j)}. \end{aligned} \tag{B.17}$$

Then, we can define the distance $D(\boldsymbol{\phi}_I, \boldsymbol{\phi}'_I)$ by using the similarity as

$$\begin{aligned} D(\boldsymbol{\phi}_I, \boldsymbol{\phi}'_I) &= \sqrt{1 - \mu^2(\boldsymbol{\phi}_I, \boldsymbol{\phi}'_I)} \\ &= \sqrt{1 - \frac{1}{N_I^2}\sum_{i\in I}\sum_{j\in I}\cos(\phi_i - \phi'_i - \phi_j + \phi'_j)}. \end{aligned} \tag{B.18}$$

Here, let us consider the orbit connecting between the pattern $\boldsymbol{\phi}_I^{(1)} = (\phi_i^{(1)})$ and the pattern $\boldsymbol{\phi}_I^{(2)} = (\phi_i^{(2)})$ for $i \in I$, and let $\boldsymbol{\phi}_I = (\phi_i)$ for $i \in I$ represents the phase pattern on the orbit. By an analogy of the way for determining a geodesic line connecting between some certain points in the Euclidean space, and by considering the rotational symmetry of the system, we introduce the definition of the orbit, by using a parameter s specifying a position on it, as

$$z_i = C_i(s)[(1-s)z_i^{(1)} + sz_i^{(2)}],\ i \in I, \tag{B.19}$$

where

$$\begin{aligned} z_i &= \exp[\mathrm{i}(\phi_i - \theta)], \\ z_i^{(k)} &= \exp[\mathrm{i}(\phi_i^{(k)} - \theta^{(k)})],\ k = 1, 2, \end{aligned} \tag{B.20}$$

and θ and $\theta^{(k)}$ for $k = 1, 2$ are defined as follows:

$$\begin{aligned} r\exp[\mathrm{i}\theta] &= \frac{1}{N_I}\sum_{i\in I}\exp[\mathrm{i}\phi_i], \\ r^{(k)}\exp[\mathrm{i}\theta^{(k)}] &= \frac{1}{N_I}\sum_{i\in I}\exp[\mathrm{i}\phi_i^{(k)}],\ k = 1, 2, \end{aligned} \tag{B.21}$$

as explained in section 3.2.3. Here, $C_i(s)$ is a coefficient for keeping $z_i z_i^* = 1$, where the suffix $*$ is for taking a complex conjugate. It should be noted that the orbit defined by the eq. (B.19) is invariant under the rotational operation, which is the reason for introducing the definition. From the eqs. (B.19) and (B.20), we can obtain

$$\phi_i = \tan^{-1}\left[\frac{(1-s)\sin(\phi_i^{(1)}-\theta^{(1)}) + s\sin(\phi_i^{(2)}-\theta^{(2)})}{(1-s)\cos(\phi_i^{(1)}-\theta^{(1)}) + s\cos(\phi_i^{(2)}-\theta^{(2)})}\right], \; i \in I, \tag{B.22}$$

where the parameter θ is set at zero, and it is all right because of the rotational symmetry. The above expression (eq. (B.22)) is the desirable definition of the orbit.

C Details of Calculations in Chapter 4

C·1 Stationary Analysis

Here, the derivation of eqs. (4.5)-(4.7) and eq. (4.11) will be shown. By substituting eq. (4.3) into eq. (4.1), we obtain

$$\frac{\mathrm{d}\phi_i}{\mathrm{d}t} = \omega_i + \mathrm{Im}[\exp(-\mathrm{i}\phi_i)(m + Z_i)], \quad i = 1, \cdots, N, \tag{C.1}$$

where

$$m\ (= m^1) = \frac{1}{N}\sum_{j=1}^{N} \exp(\mathrm{i}\phi_j), \tag{C.2}$$

$$Z_i = \frac{1}{N}\sum_{\mu}{}' \sum_{j}{}' \exp(\mathrm{i}(\phi_j + \theta_i^\mu - \theta_j^\mu)), \quad i = 1, \cdots, N. \tag{C.3}$$

Note that we assumed $\theta_i^1 = 0$, $i = 1, \cdots N$, without loss of generality. Furthermore, m can be assumed to be a real variavle because of the rotational symmetry of the system concerned. Here, $\sum_\mu{}'$ $(= \sum_{\mu=2}^{p})$ denotes the summation over all the embedded patterns except the 1-st pattern, and $\sum_j{}'$ denotes the summation over all the oscillators except the i-th oscillator. The term Z_i can be considered as a random variable statistical independent of Z_j for $j \neq i$. By the central limit theorem, it can be regarded as normally distributed with

$$E[Z_i] = 0, \quad E[Z_i Z_j^*] = 2\sigma^2 \delta_{ij}, \quad i, j = 1, \cdots, N, \tag{C.4}$$

where $E[\,\cdot\,]$ denotes expectaion. Let us concern the macroscopic stationary state, in which the following equations

$$\omega_i + \mathrm{Im}[\exp(-\mathrm{i}\phi_i)(m + Z_i)] = 0, \quad i \in S, \tag{C.5}$$

$$\omega_i + \langle \mathrm{Im}[\exp(-\mathrm{i}\phi_i)(m + Z_i)] \rangle_t = \tilde{\omega}_i, \quad i \in D \tag{C.6}$$

hold, where S denotes a set of numbers of oscillators which phases are phase-locked (synchronized) and D denotes a set of numbers of oscillators which phases are not locked (desynchronized). The operator $\langle\,\cdot\,\rangle_t$ means the averaging operation with respect to time over sufficiently long period. The effective (angular) frequency of a desynchronized oscillator $\tilde{\omega}_i$, $i \in D$ is defined as

$$\tilde{\omega}_i = \langle \frac{\mathrm{d}\phi_i}{\mathrm{d}t} \rangle_t, \quad i \in D. \tag{C.7}$$

We can rewrite the eq. (4.1) as

$$\frac{\mathrm{d}\phi_i}{\mathrm{d}t} = \omega_i + |A_i| \sin(\arg A_i - \phi_i), \quad i = 1, \cdots, N, \tag{C.8}$$

where $A_i = m + Z_i$. It can be easily found that the oscillators belonging to the synchronized set S suffices $|\omega_i| \leq |A_i|$ for $i \in S$ and those belonging to the desynchronized set D suffices $|\omega_i| > |A_i|$ for $i \in D$. Note that A_i can be considered as a constant value with respect to time. By eq. (C.5), we obtain

$$\exp(\mathrm{i}\phi_i) = \frac{A_i}{|A_i|}\exp\left(\mathrm{i}\sin^{-1}\frac{\omega_i}{|A_i|}\right), \quad i \in S. \tag{C.9}$$

Hence, eq. (C.2) can be rewritten as

$$m = \frac{1}{N}\sum_{j\in S}\frac{A_j}{|A_j|}\exp\left(\mathrm{i}\sin^{-1}\frac{\omega_j}{|A_j|}\right) + \frac{1}{N}\sum_{j\in D}\exp(\mathrm{i}\phi_j). \tag{C.10}$$

The second term of the right-hand side of the above equation can be expected to be neglected for large N. Let us replace the summation in eq. (C.10) with expectation under a constraint of $|\omega| \le |A|$ as

$$m = E\left[\frac{A}{|A|}\exp\left(\mathrm{i}\sin^{-1}\frac{\omega}{|A|}\right)\middle| |\omega| \le |A|\right], \tag{C.11}$$

where $E[\,\cdot\,||\omega| \le |A|]$ means a statistical averaging with the constraint (a conditional expectation). Let us describe the expectation operator in eq. (C.11) explicitly as

$$\begin{aligned} m &= \int_{-\infty}^{\infty}\mathrm{d}X\int_{-\infty}^{\infty}\mathrm{d}Y\frac{1}{2\pi\sigma^2}\exp(-\frac{X^2+Y^2}{2\sigma^2})\int_{-|A|}^{|A|}\mathrm{d}\omega\frac{1}{\sqrt{2\pi\gamma^2}}\exp(-\frac{\omega^2}{2\gamma^2}) \\ &\quad\times\frac{m+X+\mathrm{i}Y}{\sqrt{(m+X)^2+Y^2}}\left[\frac{\sqrt{(m+X)^2+Y^2-\omega^2}}{\sqrt{(m+X)^2+Y^2}} + \mathrm{i}\frac{\omega}{\sqrt{(m+X)^2+Y^2}}\right], \end{aligned} \tag{C.12}$$

where X and Y are the real and imaginary part of Z, respectively. By considering the symmetry of the integrated function in the above equation, it is found that only the term

$$\frac{m+X}{\sqrt{(m+X)^2+Y^2}}\sqrt{1-\frac{\omega^2}{(m+X)^2+Y^2}} \tag{C.13}$$

in the integration remains. Eventually, we can obtain the following equation by exchanging variables as $x = X/m$, $y = Y/m$, $\tilde{\sigma}^2 = \sigma^2/m^2$:

$$\begin{aligned} m &= \frac{1}{(2\pi)^{(3/2)}\gamma\tilde{\sigma}^2}\int_{-\infty}^{\infty}\mathrm{d}x\int_{-\infty}^{\infty}\mathrm{d}y\int_{-m\sqrt{(x+1)^2+y^2}}^{m\sqrt{(x+1)^2+y^2}}\mathrm{d}\omega\exp(-\frac{\omega^2}{2\gamma^2})\exp(-\frac{x^2+y^2}{2\tilde{\sigma}^2}) \\ &\quad\times\frac{x+1}{\sqrt{(x+1)^2+y^2}}\sqrt{1-\frac{\omega^2}{m^2[(x+1)^2+y^2]}}. \end{aligned} \tag{C.14}$$

Next, we will concern the overlaps m^μ for $\mu \neq 1$. By eqs. (4.4) and (C.9), we obtain the following expression:

$$\begin{aligned} m^\mu &= \frac{1}{N}\sum_{j\in S}\exp(-\mathrm{i}\theta_j^\mu)\frac{m+X_j+\mathrm{i}Y_j}{\sqrt{(m+X_j)^2+Y_j^2}}\exp\left(\mathrm{i}\sin^{-1}\frac{\omega_j}{\sqrt{(m+X_j)^2+Y_j^2}}\right), \\ &\quad \mu = 2,\cdots,p. \end{aligned} \tag{C.15}$$

Let us expand Z_j as

$$
\begin{aligned}
Z_j &= \frac{1}{N}{\sum_{\nu}}'{\sum_{k}}' \exp[\mathrm{i}(\phi_k + \theta_j^\nu - \theta_k^\nu)] \\
&= \exp(\mathrm{i}\theta_j^\mu)m^\mu + \frac{1}{N}{\sum_{\nu}}''{\sum_{k}}' \exp[\mathrm{i}(\phi_k + \theta_j^\nu - \theta_k^\nu)], \qquad \text{(C.16)}
\end{aligned}
$$

where the symbol ${\sum_\nu}''$ denotes the summation over all the embedded patterns except the 1-st and the μ-th pattern. Let us put that

$$
Z_j = Z_j^0 + \exp(\mathrm{i}\theta_j^\mu)m^\mu, \qquad \text{(C.17)}
$$

where

$$
Z_j^0 = \frac{1}{N}{\sum_{\nu}}''{\sum_{k}}' \exp[\mathrm{i}(\phi_k + \theta_j^\nu - \theta_k^\nu)]. \qquad \text{(C.18)}
$$

Equation (C.15) can be rewritten as follows:

$$
\begin{aligned}
m^\mu &= \frac{1}{N}\sum_{j\in S} \exp(\mathrm{i}\theta_j^\mu) f(X_j, Y_j, \omega_j) \\
&= \frac{1}{N}\sum_{j\in S} \exp(\mathrm{i}\theta_j^\mu)\{f(X_j^0, Y_j^0, \omega_j) + \mathrm{Re}[\exp(\mathrm{i}\theta_j^\mu)m^\mu] f_X(X_j^0, Y_j^0, \omega_j) \\
&\quad + \mathrm{Im}[\exp(\mathrm{i}\theta_j^\mu)m^\mu] f_Y(X_j^0, Y_j^0, \omega_j)\}, \quad \mu = 2, \cdots, p, \qquad \text{(C.19)}
\end{aligned}
$$

where

$$
f(X, Y, \omega) = \frac{m + X + \mathrm{i}Y}{\sqrt{(m+X)^2 + Y^2}} \exp\left(\mathrm{i}\sin^{-1}\frac{\omega}{\sqrt{(m+X)^2+Y^2}}\right), \qquad \text{(C.20)}
$$

$$
f_X(X_j^0, Y_j^0, \omega_j) = \left.\frac{\partial}{\partial X} f(X, Y, \omega)\right|_{X=X_j^0, Y=Y_j^0}, \qquad \text{(C.21)}
$$

$$
f_Y(X_j^0, Y_j^0, \omega_j) = \left.\frac{\partial}{\partial Y} f(X, Y, \omega)\right|_{X=X_j^0, Y=Y_j^0}. \qquad \text{(C.22)}
$$

It is found that

$$
m^\mu = \frac{1}{JN}\sum_{j\in S} \exp(-\mathrm{i}\theta_j^\mu) f(X_j^0, Y_j^0, \omega_j), \quad \mu = 2, \cdots, p, \qquad \text{(C.23)}
$$

where

$$
\begin{aligned}
J &= 1 - \frac{1}{N}\sum_{j\in S} \exp[-\mathrm{i}(\theta_j^\mu + \arg m^\mu)][\cos(\theta_j^\mu + \arg m^\mu) f_X(X_j^0, Y_j^0, \omega_j) \\
&\quad + \sin(\theta_j^\mu + \arg m^\mu) f_X(X_j^0, Y_j^0, \omega_j)]. \qquad \text{(C.24)}
\end{aligned}
$$

By replacing the summation in the above equation with a statistical averaging, we can obtain

$$\begin{aligned} J &= 1 - \frac{1}{2(2\pi)^{(3/2)}\gamma\tilde{\sigma}^4 m}\int_{-\infty}^{\infty}\mathrm{d}x\int_{-\infty}^{\infty}\mathrm{d}y\int_{-m\sqrt{(x+1)^2+y^2}}^{m\sqrt{(x+1)^2+y^2}}\mathrm{d}\omega\exp(-\frac{\omega^2}{2\gamma^2}) \\ &\quad\times\exp(-\frac{x^2+y^2}{2\tilde{\sigma}^2})\frac{x^2+x+y^2}{\sqrt{(x+1)^2+y^2}}\sqrt{1-\frac{\omega^2}{m^2[(x+1)^2+y^2]}}. \end{aligned} \tag{C.25}$$

Note that Z_i can be expressed as

$$Z_i = \sum_{\mu}{}' \exp(\mathrm{i}\theta_i^{\mu})m^{\mu}. \tag{C.26}$$

By substituting eq. (C.23) into the above, we obtain the following:

$$Z_i = \frac{1}{JN}\sum_{\mu}{}'\sum_{j\in S}\exp[\mathrm{i}(\theta_i^{\mu}-\theta_j^{\mu})]f(X_j,Y_j,\omega_j), \tag{C.27}$$

where we replaced X_j^0 and Y_j^0 with X_j and Y_j, respectively, because the difference between X_j^0 (Y_j^0) and X_j (Y_j) is of order $O(1/\sqrt{N})$. It is found that

$$\begin{aligned} 2\sigma^2 &= E[|Z_i|^2] \\ &= \frac{1}{J^2N^2}E[\sum_{\mu}{}'\sum_{\mu'}{}'\sum_{j\in S}\sum_{j'\in S}\exp[\mathrm{i}(\theta_i^{\mu}-\theta_j^{\mu}-\theta_i^{\mu'}+\theta_{j'}^{\mu'})] \\ &\quad\times f(X_j,Y_j,\omega_j)f^*(X_{j'},Y_{j'},\omega_{j'})] \\ &= \frac{1}{J^2N^2}E[\sum_{\mu}{}'\sum_{j\in S}1\,] \\ &= \frac{\alpha}{J^2}\int_{-\infty}^{\infty}\mathrm{d}X\int_{-\infty}^{\infty}\mathrm{d}Y\frac{1}{2\pi\sigma^2}\exp(-\frac{X^2+Y^2}{2\sigma^2})\int_{-|A|}^{|A|}\mathrm{d}\omega\frac{1}{\sqrt{2\pi\gamma^2}}\exp(-\frac{\omega^2}{2\gamma^2}). \end{aligned} \tag{C.28}$$

Finally, we can get

$$\begin{aligned} \tilde{\sigma}^4 &= \frac{\alpha}{2(2\pi)^{3/2}\gamma m^2 J^2}\int_{-\infty}^{\infty}\mathrm{d}x\int_{-\infty}^{\infty}\mathrm{d}y\int_{-m\sqrt{(x+1)^2+y^2}}^{m\sqrt{(x+1)^2+y^2}}\mathrm{d}\omega \\ &\quad\times\exp(-\frac{\omega^2}{2\gamma^2})\exp(-\frac{x^2+y^2}{2\tilde{\sigma}^2}). \end{aligned} \tag{C.29}$$

Equations (C.14), (C.25) and (C.29) are corresponding to eqs. (4.5), (4.6) and (4.7), respectively. Note that on behalf of the variable J, we used M as an unknown variable which is defined as

$$M = \frac{1}{2\tilde{\sigma}^2}\hat{I}_{m,\tilde{\sigma},\gamma}\left[\frac{x^2+x+y^2}{\sqrt{(x+1)^2+y^2}}h_m(x,y,\omega)\right], \tag{C.30}$$

where

$$\widehat{I}_{m,\widetilde{\sigma},\gamma}[\,\cdot\,] = \frac{1}{(2\pi)^{3/2}\gamma\widetilde{\sigma}^2}\int_{-\infty}^{\infty}dx\int_{-\infty}^{\infty}dy\int_{-m\sqrt{(x+1)^2+y^2}}^{m\sqrt{(x+1)^2+y^2}}d\omega \times \exp(-\frac{\omega^2}{2\gamma^2})\exp(-\frac{x^2+y^2}{2\widetilde{\sigma}^2})[\,\cdot\,], \tag{C.31}$$

$$h_m(x,y,\omega) = \sqrt{1-\frac{\omega^2}{m^2[(x+1)^2+y^2]}}. \tag{C.32}$$

Hence, eqs. (C.14) and (C.29) can be rewritten as

$$m = \widehat{I}_{m,\widetilde{\sigma},\gamma}\left[\frac{x+1}{\sqrt{(x+1)^2+y^2}}h_m(x,y,\omega)\right] \tag{C.33}$$

and

$$\widetilde{\sigma}^2 = \frac{\alpha}{2(m-M)^2}\widehat{I}_{m,\widetilde{\sigma},\gamma}[1], \tag{C.34}$$

respectively.

C·2 Derivation of the Effective Frequency Distribution

The effective (angular) frequency distribution in desynchronized oscillators is expressed by the distribution function $G_D(\widetilde{\omega})$ defined as

$$G_D(\widetilde{\omega})\Delta\widetilde{\omega} = \frac{1}{N}\times(\text{the number of oscillators sufficing } \ \widetilde{\omega}\le\widetilde{\omega}_i<\widetilde{\omega}+\Delta\widetilde{\omega},\ \ i\in D), \tag{C.35}$$

where $|\Delta\widetilde{\omega}|\ll 1$.

From eq. (C.6) and eq. (C.8), the relation

$$\widetilde{\omega}_i = \sqrt{\omega_i^2-|A_i|^2},\quad i\in D \tag{C.36}$$

is obtained.

Equation (C.35) can also be expressed as

$$G_D(\widetilde{\omega})\Delta\widetilde{\omega} = E[\mathrm{Prob}\{\widetilde{\omega}[\omega]\le\widetilde{\boldsymbol{\omega}}<\widetilde{\omega}[\omega]+\Delta\widetilde{\omega}\mid|\omega|>|A|\}], \tag{C.37}$$

where $\widetilde{\boldsymbol{\omega}}$ is a dummy random variable, and

$$\widetilde{\omega}[\omega] = \sqrt{\omega^2-|A|^2}. \tag{C.38}$$

Equation (C.37) can be rewritten as

$$G_D(\widetilde{\omega}) = E\left[g(\omega[\widetilde{\omega}])\left|\frac{\mathrm{d}}{\mathrm{d}\widetilde{\omega}}\omega[\widetilde{\omega}]\right|\right], \tag{C.39}$$

where $g(\omega)$ is the distribution function of the natural frequencies defined as

$$g(\omega) = \frac{1}{\sqrt{2\pi\gamma^2}} \exp(-\frac{\omega^2}{2\gamma^2}), \tag{C.40}$$

and ω is regarded as a function of $\widetilde{\omega}$ as

$$\omega[\widetilde{\omega}] = \sqrt{\widetilde{\omega}^2 + |A|^2}. \tag{C.41}$$

Therefore, the explicit expression of the distribution function of the effective frequencies of the desynchronized oscillators can be obtained as

$$\begin{aligned} G_D(\widetilde{\omega}) &= E\left[\frac{1}{\sqrt{2\pi\gamma^2}} \exp(-\frac{\widetilde{\omega}^2 + |A|^2}{2\gamma^2}) \frac{|\widetilde{\omega}|}{\sqrt{\widetilde{\omega}^2 + |A|^2}}\right] \\ &= \frac{1}{2\pi\sigma^2} \frac{1}{\sqrt{2\pi\gamma^2}} \int_{-\infty}^{\infty} \mathrm{d}X \int_{-\infty}^{\infty} \mathrm{d}Y \exp(-\frac{X^2 + Y^2}{2\sigma^2}) \\ &\quad \times \exp[-\frac{\widetilde{\omega}^2 + (m+X)^2 + Y^2}{2\gamma^2}] \frac{|\widetilde{\omega}|}{\sqrt{\widetilde{\omega}^2 + (m+X)^2 + Y^2}} \\ &= \frac{1}{(2\pi)^{3/2}\gamma\widetilde{\sigma}^2} \int_0^{\infty} \mathrm{d}R \int_0^{2\pi} \mathrm{d}\theta \exp(-\frac{R^2 - 2R\cos\theta + 1}{2\widetilde{\sigma}^2}) \\ &\quad \times \exp(-\frac{\widetilde{\omega}^2 + m^2R^2}{2\gamma^2}) \frac{R|\widetilde{\omega}|}{\sqrt{\widetilde{\omega}^2 + m^2R^2}}. \end{aligned} \tag{C.42}$$

The effective frequency distribution in synchronized oscillators is described by a function $G_S(\widetilde{\omega})$ which is explicitly expressed as follows:

$$\begin{aligned} G_S(\widetilde{\omega}) &= \delta(\widetilde{\omega}) \frac{1}{N} \sum_{j \in S} 1 \\ &= \widehat{I}_{m,\widetilde{\sigma},\gamma}[1] \delta(\widetilde{\omega}). \end{aligned} \tag{C.43}$$

C·3 Derivations of $F_\beta(m)$ and $G_\beta(m)$

By differentiating an equality concerning with the Bessel function:

$$I_0(\sqrt{a^2 - b^2}) = \frac{1}{2\pi}\int_{-\pi}^{\pi} e^{a\cos\phi}\cos(b\sin\phi)\mathrm{d}\phi, \tag{C.44}$$

with respect to a and b, and combining the resultants, we get

$$\frac{a+b}{\sqrt{a^2 - b^2}} I_1(\sqrt{a^2 - b^2}) = \frac{1}{2\pi}\int_{-\pi}^{\pi} e^{a\cos\phi}\cos(\phi - b\sin\phi)\mathrm{d}\phi. \tag{C.45}$$

Here, $I_0(\cdot)$ and $I_1(\cdot)$ are the modified Bessel functions of the zero-th and the 1-st order, respectively. Hence, we can get eq. (4.26), by using that

$$\begin{aligned} F_\beta(m) &= E[\cos(\phi - b\sin\phi)] \\ &= \int \rho_m(\phi)\cos(\phi - b\sin\phi)\mathrm{d}\phi \\ &= \frac{1}{2\pi I_0(a)}\int_{-\pi}^{\pi} e^{a\cos\phi}\cos(\phi - b\sin\phi)\mathrm{d}\phi, \end{aligned} \tag{C.46}$$

where $b = \beta m$, under the condition that the phases are unimodally distributed as expressed by eq. (4.24).

In Appendix C·4, $G_\beta(m)$ will be introduced as

$$\begin{aligned} G_\beta(m) &= E[\cos(b\sin\phi)] \\ &= \int \rho_m(\phi)\cos(b\sin\phi)\mathrm{d}\phi \\ &= \frac{1}{2\pi I_0(a)}\int_{-\pi}^{\pi} e^{a\cos\phi}\cos(b\sin\phi)\mathrm{d}\phi. \end{aligned} \tag{C.47}$$

The above and eq. (C.44) lead to eq. (4.29).

C·4 Time Evolution Equation of $\sigma^2(t)$

Here, we derive the macroscopic time evolution equation of $\sigma^2(t)$. The procedure to be shown is similar to that for the spin-glass neural network model for associative memory. [61, 78] However, the introduction of the distribution density function of phases is necessary in our model because phases take continuous values. Moreover, it is also necessary to introduce an appropriate density operator (which will be mentioned below) for statistical calculations of correlating variables. Actually, the necessity of the density operator arises from a certain mathematical structure of the basic equation of the system concerned.

Let us start with the expression:

$$\begin{aligned} 2\sigma^2(t) &= E[|Z_i(t)|^2] \\ &= E[|\frac{1}{N}\sum_{\mu}{}'\sum_{j}{}' \exp[\mathrm{i}(\phi_j(t) + \theta_i^\mu - \theta_j^\mu)]|^2] \\ &= \frac{1}{N^2}\sum_{j}{}'\sum_{j'}{}'\sum_{\mu}{}'\sum_{\mu'}{}' E[z_{ij\mu}(t) z^*_{ij'\mu'}(t)], \end{aligned} \tag{C.48}$$

where

$$z_{ij\mu}(t) = \exp[\mathrm{i}(\phi_j(t) + \theta_i^\mu - \theta_j^\mu)]. \tag{C.49}$$

The summation in eq. (C.48) can be decomposed into the following four types: (i): $j = j'$ and $\mu = \mu'$, in which there are $(N-1)(p-1)$ terms, and

$$E[|z_{ij\mu}(t)|^2] = 1. \tag{C.50}$$

(ii): $j = j'$ and $\mu \neq \mu'$, in which there are $(N-1)(p-1)(p-2)$ terms, and

$$E[z_{ij\mu}(t) z^*_{ij\mu'}(t)] = 0. \tag{C.51}$$

(iii): $j \neq j'$ and $\mu = \mu'$, in which there are $(N-1)(N-2)(p-1)$ terms, and we put

$$v(t) = E[z_{ij\mu}(t) z^*_{ij'\mu}(t)]. \tag{C.52}$$

(iv): $j \neq j'$ and $\mu \neq \mu'$, in which there are $(N-1)(N-2)(p-1)(p-2)$ terms, and we put

$$w(t) = E[z_{ij\mu}(t) z^*_{ij'\mu'}(t)]. \tag{C.53}$$

Let us consider the case of $N \gg 1$. Hence, we have

$$2\sigma^2(t) = \alpha + V(t) + W(t), \tag{C.54}$$

where

$$V(t) = \alpha N v(t), \quad W(t) = \alpha^2 N^2 w(t). \tag{C.55}$$

Here, we concern $v(t)$. Let us put as

$$\phi(t) = \phi_j(t), \ \phi'(t) = \phi_{j'}(t), \ \theta = \theta_j^\mu, \ \theta' = \theta_{j'}^\mu. \tag{C.56}$$

From $Z(t)$ and $Z'(t)$ we extract the terms including θ and θ' (which are correlated to ϕ and ϕ', respectively) as

$$\begin{aligned} Z(t) &= Q(t) + \exp(\mathrm{i}\theta)R(t) \\ &\quad + \frac{1}{N}\exp[\mathrm{i}(\theta - \theta' + \phi'(t))], \end{aligned} \tag{C.57}$$

$$\begin{aligned} Z'(t) &= Q'(t) + \exp(\mathrm{i}\theta')R(t) \\ &\quad + \frac{1}{N}\exp[\mathrm{i}(\theta' - \theta + \phi(t))], \end{aligned} \tag{C.58}$$

where

$$Q(t) = \frac{1}{N}\sum_\nu{}'' \sum_k{}' \exp[\mathrm{i}(\theta_j^\nu - \theta_k^\nu + \phi_k(t))], \tag{C.59}$$

$$Q'(t) = \frac{1}{N}\sum_\nu{}'' \sum_k{}' \exp[\mathrm{i}(\theta_{j'}^\nu - \theta_k^\nu + \phi_k(t))], \tag{C.60}$$

$$R(t) = \frac{1}{N}\sum_k{}'' \exp[\mathrm{i}(\phi_k(t) - \theta_k^\mu)]. \tag{C.61}$$

The symbol $\sum_\nu''$ means the summation over $\nu \neq 1$ and $\nu \neq \mu$, the symbol $\sum_k'$ the summatin over $k \neq j$, the symbol $\sum_k''$ the summation over $k \neq j$ and $k \neq j'$. The variables $Q(t)$, $Q'(t)$ and $R(t)$ can be considered to be normally distributed random variables which are statistically independent of each other and satisfying

$$E[Q(t)] = E[Q'(t)] = E[R(t)] = 0, \tag{C.62}$$

$$E[|Q(t)|^2] = E[|Q'(t)|^2] = 2\sigma^2(t), \tag{C.63}$$

$$E[|R(t)|^2] = 2\sigma^2(t)/p. \tag{C.64}$$

It should be noted that $R(t)$ means a correlation which is of order $O(1/\sqrt{N})$ between random variables ϕ and θ (ϕ' and θ'). As will be mentioned later, a proper operator will be introduced for systematic consideration for this correlation.

We have

$$\begin{aligned} v(t+1) = e^{-\beta^2\sigma^2} & E[e^{\mathrm{i}(\phi-\phi'-\theta+\theta')} \\ & \times \exp[\mathrm{i}\beta \mathrm{Im}\{e^{-\mathrm{i}\phi}[m + e^{\mathrm{i}\theta}R + \frac{1}{N}e^{\mathrm{i}(\theta-\theta'+\phi')}]\}] \\ & \times \exp[\mathrm{i}\beta \mathrm{Im}\{e^{\mathrm{i}\phi'}[m + e^{-\mathrm{i}\theta'}R^* + \frac{1}{N}e^{-\mathrm{i}(\theta'-\theta+\phi)}]\}]], \end{aligned} \tag{C.65}$$

where we have statistically averaged with respect to Q and Q'. By expanding with respect to $1/N$, and neglecting higher order terms, the expectation part can be written as

$$\begin{aligned} & E[e^{\mathrm{i}(\phi-\phi'-\theta+\theta')} \\ & \times \exp\{\mathrm{i}\beta \mathrm{Im}[e^{-\mathrm{i}\phi}(m + e^{\mathrm{i}\theta}R)]\} \exp\{\mathrm{i}\beta \mathrm{Im}[e^{\mathrm{i}\phi'}(m + e^{-\mathrm{i}\theta'}R^*)]\}] \\ & + E[e^{\mathrm{i}(\phi-\phi'-\theta+\theta')} \exp\{\mathrm{i}\beta \mathrm{Im}[e^{-\mathrm{i}\phi}m]\} \exp\{\mathrm{i}\beta \mathrm{Im}[e^{\mathrm{i}\phi'}m]\} \\ & \times \mathrm{i}\beta\frac{2}{N}\mathrm{Im}[e^{-\mathrm{i}(\phi-\phi'-\theta+\theta')}]]\}. \end{aligned} \tag{C.66}$$

For calculating the above expectation, the operator

$$\begin{aligned} \widehat{P}_v[\cdot] \ = \ & \int\int\int\int \mathrm{d}\phi \mathrm{d}\phi' \mathrm{d}\theta \mathrm{d}\theta' (\frac{1}{2\pi})^2 \rho_m(\phi)\rho_m(\phi') \\ & \times (1 + Re^{-\mathrm{i}(\phi-\theta)})(1 + R^* e^{\mathrm{i}(\phi'-\theta')})[\cdot] \end{aligned} \tag{C.67}$$

is introduced as a substitute for taking expectations with respect to ϕ, ϕ', θ and θ'. The operator satisfies

$$\widehat{P}_v[e^{\mathrm{i}(\phi-\theta)}] = R, \tag{C.68}$$

$$\widehat{P}_v[e^{-\mathrm{i}(\phi'-\theta')}] = R^*. \tag{C.69}$$

By using the operator $\widehat{P}_v$, we can systematically take account of correlations of random variables for calculations of expectations.

Let us calculate the first expectation part in eq. (C.66). By executing integrations with respect to ϕ and ϕ', we obtain

$$E[e^{-\mathrm{i}(\theta-\theta')}F_\beta(m + e^{\mathrm{i}\theta}R)F_\beta(m + e^{-\mathrm{i}\theta'}R^*) + |R|^2 G_\beta^2(m)], \tag{C.70}$$

where $G_\beta(m)$ is defined as

$$G_\beta(m) = E[\cos(\beta m \sin\phi)]. \tag{C.71}$$

Moreover, by expanding with respect to R and R^*, executing integrations with respect to θ and θ', and finally taking expectation with respect to R, we obtain the following expression for the first part in eq. (C.66):

$$[F_\beta'^2(m) + G_\beta^2(m)]\frac{2\sigma^2}{p}. \tag{C.72}$$

Next, let us calculate the second expectation part. By integrating with respect to θ, θ', ϕ and ϕ', it is found that the second part is equal to

$$\frac{\beta}{N}G_\beta^2(m). \tag{C.73}$$

From all the above, we can get the following result:

$$\begin{aligned} &V(t+1) = \\ &\quad 2e^{-\beta^2\sigma^2(t)}\{(F_\beta'^2[m(t)] + G_\beta^2[m(t)])\sigma^2 \\ &\quad +\frac{1}{2}\alpha\beta G_\beta^2[m(t)]\}. \end{aligned} \tag{C.74}$$

Next, we concern $w(t)$ in a similar manner. Let us put as

$$\begin{aligned} &\phi(t) = \phi_j(t),\ \phi'(t) = \phi_{j'}(t),\ \tilde{\phi}(t) = \phi_i(t), \\ &\theta = \theta_j^\mu,\ \theta' = \theta_{j'}^{\mu'},\ \tilde{\theta} = \theta_i^\mu,\ \tilde{\theta}' = \theta_i^{\mu'}, \end{aligned} \tag{C.75}$$

$$Z(t) = Q(t) + \frac{1}{N}\exp[\mathrm{i}(\theta - \tilde{\theta} + \tilde{\phi}(t))], \tag{C.76}$$

$$Z'(t) = Q'(t) + \frac{1}{N}\exp[\mathrm{i}(\theta' - \tilde{\theta}' + \tilde{\phi}(t))], \tag{C.77}$$

$$\begin{aligned} Q(t) &= \frac{1}{N}\sum_{\nu(\neq 1,\mu)}\sum_{k(\neq j)}\exp[\mathrm{i}(\theta_j^\nu - \theta_k^\nu + \phi_k(t))] \\ &\quad + \exp(\mathrm{i}\theta)R(t) \end{aligned} \tag{C.78}$$

$$\begin{aligned} Q'(t) &= \frac{1}{N}\sum_{\nu(\neq 1,\mu')}\sum_{k(\neq j')}\exp[\mathrm{i}(\theta_{j'}^\nu - \theta_k^\nu + \phi_k(t))] \\ &\quad + \exp(\mathrm{i}\theta')R'(t) \end{aligned} \tag{C.79}$$

$$R(t) = \frac{1}{N}\sum_{k(\neq j,i)}\exp[\mathrm{i}(\phi_k(t) - \theta_k^\mu)], \tag{C.80}$$

$$R'(t) = \frac{1}{N}\sum_{k(\neq j',i)}\exp[\mathrm{i}(\phi_k(t) - \theta_k^{\mu'})]. \tag{C.81}$$

Variables $Q(t)$ and $Q'(t)$ can be regarded as normaly distributed random variables statistically independent of each other, and satisfying

$$E[Q(t)] = E[Q'(t)] = 0, \tag{C.82}$$

$$E[|Q(t)|^2] = E[|Q'(t)|^2] = 2\sigma^2(t). \tag{C.83}$$

Variables $R(t)$ and $R'(t)$ are also random variables statistically independent of each other, and satisfying

$$E[R(t)] = E[R'(t)] = 0, \tag{C.84}$$

$$E[|R(t)|^2] = E[|R'(t)|^2] = 2\sigma^2(t)/p. \tag{C.85}$$

Here, let us note that $R(t)$ means a correlation between ϕ and θ (or between $\tilde{\phi}$ and $\tilde{\theta}$). $R'(t)$ means a correlation between ϕ' and θ' (or between $\tilde{\phi}$ and $\tilde{\theta}'$).

We have

$$\begin{aligned} w(t+1) = e^{-\beta^2\sigma^2} & E[e^{\mathrm{i}(\phi-\phi'+\tilde{\theta}-\theta-\tilde{\theta}'+\theta')} \\ & \times \exp\{\mathrm{i}\beta \mathrm{Im}[e^{-\mathrm{i}\phi}(m+\frac{1}{N}e^{\mathrm{i}(\theta-\tilde{\theta}+\tilde{\phi})})]\} \\ & \times \exp\{\mathrm{i}\beta \mathrm{Im}[e^{\mathrm{i}\phi'}(m+\frac{1}{N}e^{-\mathrm{i}(\theta'-\tilde{\theta}'+\tilde{\phi})})]\}, \end{aligned} \tag{C.86}$$

where we have statistically averaged with respect to Q and Q'. For calculating the expectation in the above equation, the operator

$$\begin{aligned} & \widehat{P}_w[\cdot] = \\ & \int\!\!\int\!\!\int\!\!\int\!\!\int\!\!\int\!\!\int \mathrm{d}\phi \mathrm{d}\phi' \mathrm{d}\tilde{\phi} \mathrm{d}\theta \mathrm{d}\theta' \mathrm{d}\tilde{\theta} \mathrm{d}\tilde{\theta}' (\frac{1}{2\pi})^4 \rho_m(\phi)\rho_m(\phi')\rho_m(\tilde{\phi}) \\ & \times(1+Re^{-\mathrm{i}(\phi-\theta)})(1+R'^{*}e^{\mathrm{i}(\phi'-\theta')}) \\ & \times(1+R'e^{-\mathrm{i}(\tilde{\phi}-\tilde{\theta}')})(1+R^{*}e^{\mathrm{i}(\tilde{\phi}-\tilde{\theta})})[\cdot] \end{aligned} \tag{C.87}$$

is introduced as a substitute for taking expectations with respect to ϕ, ϕ', $\tilde{\phi}$, θ, θ', $\tilde{\theta}$ and $\tilde{\theta}'$. The operator satisfies

$$\widehat{P}_w[e^{\mathrm{i}(\phi-\theta)}] = R, \tag{C.88}$$

$$\widehat{P}_w[e^{-\mathrm{i}(\phi'-\theta')}] = R'^{*}, \tag{C.89}$$

$$\widehat{P}_w[e^{-\mathrm{i}(\tilde{\phi}-\tilde{\theta})}] = R^{*}, \tag{C.90}$$

$$\widehat{P}_w[e^{\mathrm{i}(\tilde{\phi}-\tilde{\theta}')}] = R'. \tag{C.91}$$

By using the operator $\widehat{P}_w$, we can systematically treat correlations of random variables for the calculations of expectations.

By integrating with respect to ϕ and ϕ', the expectation part in eq. (C.86) becomes

$$\begin{aligned} & E[e^{\mathrm{i}(\tilde{\theta}-\theta-\tilde{\theta}'+\theta')}F_\beta(m+\frac{1}{N}e^{\mathrm{i}(\theta-\tilde{\theta}+\tilde{\phi})})F_\beta(m+\frac{1}{N}e^{-\mathrm{i}(\theta'-\tilde{\theta}'+\tilde{\phi})}) \\ & +RR'^{*}e^{\mathrm{i}(\tilde{\theta}-\tilde{\theta}')}G_\beta(m+\frac{1}{N}e^{\mathrm{i}(\theta-\tilde{\theta}+\tilde{\phi})})G_\beta(m+\frac{1}{N}e^{-\mathrm{i}(\theta'-\tilde{\theta}'+\tilde{\phi})})]. \end{aligned} \tag{C.92}$$

By expanding with respect to $1/N$, neglecting higher order terms (higher than $(1/N)^2$), and integrating with respect to θ, θ', $\tilde{\theta}$, $\tilde{\theta}'$ and $\tilde{\phi}$, we obtain

$$w(t+1) = e^{-\beta^2\sigma^2}(E[|R|^2|R'|^2]G_\beta^2(m) + \frac{1}{N^2}F_\beta'^2(m)). \tag{C.93}$$

Hence, the equation

$$W(t+1) = 2e^{-\beta^2\sigma^2(t)}\{2G_\beta^2[m(t)]\sigma^4(t) + \frac{\alpha^2}{2}F_\beta'^2[m(t)]\}. \tag{C.94}$$

is obtained. Finally, we get the time evolution equation of the macroscopic variable $\sigma^2(t)$ as

$$\begin{aligned}\sigma^2(t+1) &= \frac{\alpha}{2} + e^{-\beta^2\sigma^2(t)}\{2G_\beta^2[m(t)]\sigma^4(t) \\ &\quad +(F_\beta'^2[m(t)] + G_\beta^2[m(t)])\sigma^2(t) \\ &\quad +\frac{1}{2}\alpha\beta G_\beta^2[m(t)]\},\end{aligned} \tag{C.95}$$

where the term including $\alpha^2 \ll 1$ is neglected.

C·5 Macrodynamics with the Distribution of Natural Frequencies

Let us consider the case that the natural frequencies are normally distributed with

$$E[\omega_i] = 0, \quad E[\omega_i\omega_j] = \gamma^2\delta_{ij}, \tag{C.96}$$

and that ω_i is statistically independent of $\{\theta_i^\mu\}$. Hence,

$$\begin{aligned}m(t+1) &= E[\exp(\mathrm{i}\omega_i)]E[\exp[\mathrm{i}\phi_i(t)] \\ &\quad \times\exp\{\mathrm{i}\beta\mathrm{Im}[\exp[-\mathrm{i}\phi_i(t)][m(t)+Z_i(t)]]\}] \\ &= e^{-[\gamma^2+\beta^2\sigma^2(t)]/2}F_\beta[m(t)].\end{aligned} \tag{C.97}$$

Similarly, the time evolution equation for $\sigma^2(t)$ can be obtained as

$$\begin{aligned}\sigma^2(t+1) &= \frac{\alpha}{2} + e^{-[\gamma^2+\beta^2\sigma^2(t)]} \\ &\quad \times\{2G_\beta^2[m(t)]\sigma^4(t) \\ &\quad +(F_\beta'^2[m(t)] + G_\beta^2[m(t)])\sigma^2(t) \\ &\quad +\frac{1}{2}\alpha\beta G_\beta^2[m(t)]\},\end{aligned} \tag{C.98}$$

with $\sigma^2(0) = \alpha/2$.

References

1) G. Nicolis and I. Prigogine: *Self-Organization in Nonequilibrium systems* (John Wiley & Sons, New York, 1977).

2) H. Haken: *Synergetics–An Introduction* (Springer-Verlag, Berlin, 1978).

3) H. Haken: *Advanced Synergetics: Instability Hierarchies of Self-Organizing Systems and Devices* (Springer-Verlag, Berlin, 1983).

4) Y. Kuramoto: *Chemical Oscillations, Waves, and Turbulences* (Springer, Berlin, 1984).

5) H. Hayashi, S. Ishizuka, M. Ohta and K. Hirakawa: Phys. Lett. A **88** (1982) 435.

6) H. Hayashi and S. Ishizuka: J. Theor. Biol. **156** (1992) 269.

7) K. Aihara, G. Matsumoto and M. Ichikawa: Phys. Lett. A **111** (1985) 251.

8) N. Takahashi, Y. Hanyu, T. Musha, R. Kubo and G. Matsumoto: Physica D **43** (1990) 318.

9) H. Hayashi and S. Ishizuka: *Physics of the Living State* ed. T. Musha and Y. Sawada (Ohmsha and IOS Press, Tokyo, Amsterdam, 1994) p. 193.

10) H. Hayashi and S. Ishizuka: Brain Res. **686** (1995) p. 194.

11) S. J. Schiff, K. Jerger, D. H. Duong, T. Chang, M. L. Spano and W. L. Ditto: Nature **370** (1994) 615.

12) C. M. Gray, P. König, A. K. Engel and W. Singer: Nature **338** (1989) 334.

13) C. M. Gray and W. Singer: Proc. Natl. Acad. Sci. USA **86** (1989) 1698.

14) W. J. Freeman: Biol. Cybern. **56** (1987) 139.

15) C. A. Skarda and W. J. Freeman: Behavioral Brain Sci. **10** (1987) 161.

16) A. Babloyantz, J. M. Salazar and C. Nicolis: Phys. Lett. A **111** (1985) 152.

17) R. Eckhorn: *Neuronal Cooperativity* ed. J. Krüger (Springer, Berlin, 1991) p. 184.

18) C. M. Gray: *1992 Lectures in Complex Systems* ed. L. Nadal and D. L. Stein (Addison-Wesley, USA, 1993) p. 89.

19) H. Degn, A. V. Holden and L. F. Olsen (ed.): *Chaos in Biological Systems* (Plenum Press, New York, 1987).

20) D. Duke and W. Prichard (ed.): *Measuring Chaos in the Human Brain* (World Scientific, Singapore, 1991).

21) H. Hayashi and S. Ishizuka: *Noise in Physical Systems and 1/f Fluctuations* ed. T. Musha, S. Sato and M. Yamamoto (Ohmsha, Tokyo, 1991) p. 497.

22) H. G. Schuster: *Deterministic Chaos An Introduction* (3rd ed.) (VCH, Germany, 1995).

23) S. J. Shenker: Physica D **5** (1982) 405.

24) M. H. Jensen, P. Bak and T. Bohr: Phys. Rev. Lett. **50** (1983) 1637.

25) M. H. Jensen, P. Bak and T. Bohr: Phys. Rev. A **30** (1984) 1960.

26) T. Bohr, P. Bak and M. H. Jensen: Phys. Rev. A **30** (1984) 1970.

27) H. Sompolinsky, D. Golomb and D. Kleinfeld: Phys. Rev. A **43** (1991) 6990.

28) Y. Kuramoto, T. Aoyagi, I. Nishikawa, T. Chawanya and K. Okuda: Prog. Theor. Phys. **87** (1992) 1119.

29) H. Shimizu and Y. Yamaguchi: Prog. Theor. Phys. Suppl. No.99 (1989) 404.

30) B. Baird: Physica D **42** (1990) 365.

31) S. Grossberg and D. Somers: Neural Networks **4** (1991) 453.

32) H. Sakaguchi: Phys. Lett. A **174** (1993) 289.

33) Y. Yao and W. J. Freeman: Neural Networks **3** (1990) 153.

34) W. J. Freeman: Physica D **75** (1994) 151.

35) B. Baird: Physica D **22** (1986) 150.

36) Y. Kuramoto and I. Nishikawa: J. Stat. Phys. **49** (1987) 569.

37) H. Daido: J. Stat. Phys. **60** (1990) 753.

38) S. H. Strogatz and R. E. Mirollo: J. Stat. Phys. : **63** (1991) 613.

39) J. Swift, S. H. Strogatz and K. Wiesenfeld: Physica D **55** (1992) 239.

40) L. L. Bonilla, J. C. Neu and R. Spigler: J. Stat. Phys. **67** (1992) 313.

41) S. Watanabe and S. H. Strogatz: Phys. Rev. Lett. **70** (1993) 2391.

42) J. L. Hemmen and W. F. Wreszinski: J. Stat. Phys. **72** (1993) 145.

43) H. Sakaguchi, S. Shinomoto and Y. Kuramoto: Prog. Theor. Phys. **79** (1988) 1069.

44) E. Niebur, H. G. Schuster, D. M. Kammen and C. Koch: Phys. Rev. A **44** (1991) 6895.

45) H. Daido: Prog. Theor. Phys. **77** (1987) 622.

46) L. L. Bonilla, C. J. P. Vicente and J. M. Rubi: J. Stat. Phys. **70** (1993) 921.

47) H. Sakaguchi: Prog. Theor. Phys. **79** (1988) 39.

48) E. Niebur, H. G. Schuster and D. M. Kammen: Phys. Rev. Lett. **67** (1991) 2753.

49) R. E. Mirollo and S. H. Strogatz: J. Stat. Phys. **60** (1990) 245.

50) G. B. Ermentrout: Physica D **41** (1990) 219.

51) P. C. Matthews, R. E. Mirollo and S. H. Strogatz: Physica D **52** (1991) 293.

52) B. Christiansen and M. T. Levinsen: Phys. Rev. E **48** (1993) 743.

53) Y. Kuramoto: Physica D **50** (1991) 15.

54) D. Hansel and H. Sompolinsky: Phys. Rev. Lett. **68** (1992) 718.

55) J. A. Sepulchre and A. Babloyantz: Phys. Rev. E **48** (1993) 945.

56) J. J. Collins and I. N. Stewart: J. Nonlinear Sci. **3** (1993) 349.

57) J. J. Collins and S. A. Richmond: Biol. Cybern. **71** (1994) 375.

58) J. J. Collins and I. Stewart: Biol. Cybern. **71** (1994) 95.

59) K. Okuda: Physica D **63** (1993) 424.

60) M. H. Hassoun: *Fundamentals of Artificial Neural Networks* (The MIT Press, Massachusetts, 1995).

61) S. Amari and K. Maginu: Neural Networks **1** (1988) 63.

62) K. Kaneko (ed.): *Theory and Applications of Coupled Map Lattices* (John Wiley & Sons, New York, 1993).

63) K. Kaneko: Physica D **54** (1991) 5.

64) T. Matsuno, Y. Kikkawa, M. Iguchi, K. Toko and K. Yamafuji: J. Phys. Soc. Jpn. **63** (1994) 1194.

65) P. Grassberger and I. Procaccia: Physica D **9** (1983) 189.

66) D. Ruelle: Proc. R. Soc. Lond. A **427** (1990) 241.

67) K. Judd: Physica D **56** (1992) 216.

68) M. Lefranc, D. Hennequin and P. Glorieux: Phys. Lett. A **163** (1992) 269.

69) F. M. Gardner: *Phaselock Techniques* (2nd ed.) (John Wiley & Sons, New York, 1979).

70) P. V. Brennan: *Phase-Locked Loops: Principles and Practice* (Macmillan, London, 1996).

71) D. D'Humieres, M. R. Beasley, B. A. Huberman and A. Libchaber: Phys. Rev. A **26** (1982) 249.

72) T. Endo and L. O. Chua: IEEE Trans. Circuits Syst. **35** (1988) 987.

73) T. Matsuno, M. Iguchi, K. Toko and K. Yamafuji: J. Phys. Soc. Jpn. **64** (1995) 1837.

74) D. H. Ackley, G. E. Hinton and T. J. Sejnowski: Cognitive Science **9** (1985) 147.

75) H. Risken: *The Fokker-Planck Equation* (Springer-Verlag, Berlin, 1989).

76) D. J. Amit, H. Gutfreund and H. Sompolinsky: Phys. Rev. Lett. **55** (1985) 1530.

77) D. J. Amit, H. Gutfreund and H. Sompolinsky: Phys. Rev. A **32** (1985) 1007.

78) S. Amari: *Neural and Synergetic Computers* ed. H. Haken (Springer-Verlag, Berlin, 1988) p. 85.

79) C. M. Marcus, F. R. Waugh and R. M. Westervelt: Phys. Rev. A **41** (1990) 3355.

80) S. Yoshizawa, M. Morita and S. Amari: Neural Networks **6** (1993) 167.

81) D. Bollé, G. M. Shim, B. Vinck and V. A. Zagrebnov: J. Stat. Phys. **74** (1994) 565.

82) D. Bollé, G. M. Shim and B. Vinck: J. Stat. Phys. **74** (1994) 583.

83) M. Shiino and T. Fukai: Phys. Rev. E **48** (1993) 867.

84) Y. Nakamura, K. Torii and T. Munakata: Phys. Rev. E **51** (1995) 1538.

85) J. Cook: J. Phys. A **22** (1989) 2057.

86) T. Matsuno, Y. Imada, K. Toko and K. Yamafuji: J. Phys. Soc. Jpn. **63** (1994) 4335.

87) T. Matsuno, K. Toko and K. Yamafuji: J. Phys. Soc. Jpn. **65** (1996) 1500.

88) D. Stassinopoulos, G. Huber and P. Alstrøm: Phys. Rev. Lett. **64** (1990) 3007.

89) D. Stassinopoulos and P. Alstrøm: Phys. Rev. A **45** (1992) 675.

90) K. Kaneko: Phys. Rev. Lett. **63** (1989) 219.

91) K. Kaneko: Physica D **41** (1990) 137.

92) L. Fabiny and K. Wiesenfeld: Phys. Rev. A **43** (1991) 2640.

93) D. Golomb, D. Hansel, B. Shraiman and H. Sompolinsky: Phys. Rev. A **45** (1992) 3516.

94) D. Hansel, G. Mato and C. Meunier: Phys. Rev. E **48** (1993) 3470.

95) K. Kaneko and T. Yomo: Physica D **75** (1994) 89.

96) D. J. Amit, H. Gutfreund and H. Sompolinsky: Phys. Rev. A **35** (1987) 2293.

97) M. Cieplak and M. S. Li: Phys. Rev. B **47** (1993) 5022.

98) S. Amari: Neural Networks **2** (1989) 451.

99) W. G. Gibson and J. Robinson: Neural Networks **5** (1992) 645.

100) I. Tsuda, E. Koerner and H. Shimizu: Prog. Theor. Phys. **78** (1987) 51.

101) I. Tsuda: Neural Networks **5** (1992) 313.

102) I. Tsuda: Physica D **75** (1994) 165.

103) F. T. Arecchi, G. Giacomelli, P. L. Ramazza and S. Residori: Phys. Rev. Lett. **65** (1990) 2531.

104) T. Aida and P. Davis: IEEE Trans. Quantum Electron. **30** (1994) 2986.

105) M. Okada: Neural Networks **8** (1995) 833.

106) S. Nara, P. Davis and H. Totsuji: Neural Networks **6** (1993) 963.

107) W. Horsthemke and R. Lefever (ed.): *Noise-Induced Transitions* (Springer, Berlin, 1984).

108) M. E. Inchiosa and A. R. Bulsara: Phys. Lett. A **200** (1995) 283.

109) P. Jung and G. M. Kress: Phys. Rev. Lett. **74** (1995) 2130.

110) J. F. Lindner, B. K. Meadows, W. L. Ditto, M. E. Inchiosa and A. R. Bulsara: Phys. Rev. Lett. **75** (1995) 3.

111) M. Morillo, J. G. Ordoñez and J. M. Casado: Phys. Rev. E **52** (1995) 316.

112) A. Bulsara, E. W. Jacobs, T. Zhou, F. Moss and L. Kiss: J. theor. Biol. **152** (1991) 531.

113) A. Longtin: J. Stat. Phys. **70** (1993) 309.

114) J. J. Collins, C. C. Chow and T. T. Imhoff: Nature **376** (1995) 236.

115) E. Ott, C. Grebogi and J. A. Yorke: Phys. Rev. Lett. **64** (1990) 1196.

116) I. Aranson, H. Levine and L. Tsimring: Phys. Rev. Lett. **72** (1994) 2561.

117) H. Gang and Q. Zhilin: Phys. Rev. Lett. **72** (1994) 68.

118) V. V. Astakhov, V. S. Anishchhenko and A. V. Shabunin: IEEE Trans. Circuits Syst. **42** (1995) 352.

119) G. A. Johnson, M. Löcher and E. R. Hunt: Phys. Rev. E **51** (1995) 1625.

120) M. J. Feigenbaum, L. P. Kadanoff and S. J. Shenker: Physica D **5** (1982) 370.

121) S. Ostlund, D. Rand, J. Sethna and E. Siggia: Physica D **8** (1983) 303.

122) K. Kaneko: Prog. Theor. Phys. **72** (1984) 1089.

123) M. H. Jensen, L. P. Kadanoff, A. Libchaber, I. Procaccia and J. Stavans: Phys. Rev. Lett. **55** (1985) 2798.

124) G. M. Zaslavsky: Phys. Lett. A **69** (1978) 145.

125) D. Rand, S. Ostlund, J. Sethna and E. D. Siggia: Phys. Rev. Lett. **49** (1982) 132.

126) M. H. Jensen and I. Procaccia: Phys. Rev. A **32** (1985) 1225.

127) W. Wenzel, O. Biham and C. Jayaprakash: Phys. Rev. A **43** (1991) 6550.

128) S. Y. Kim and B. Hu: Phys. Rev. A **44** (1991) 934.

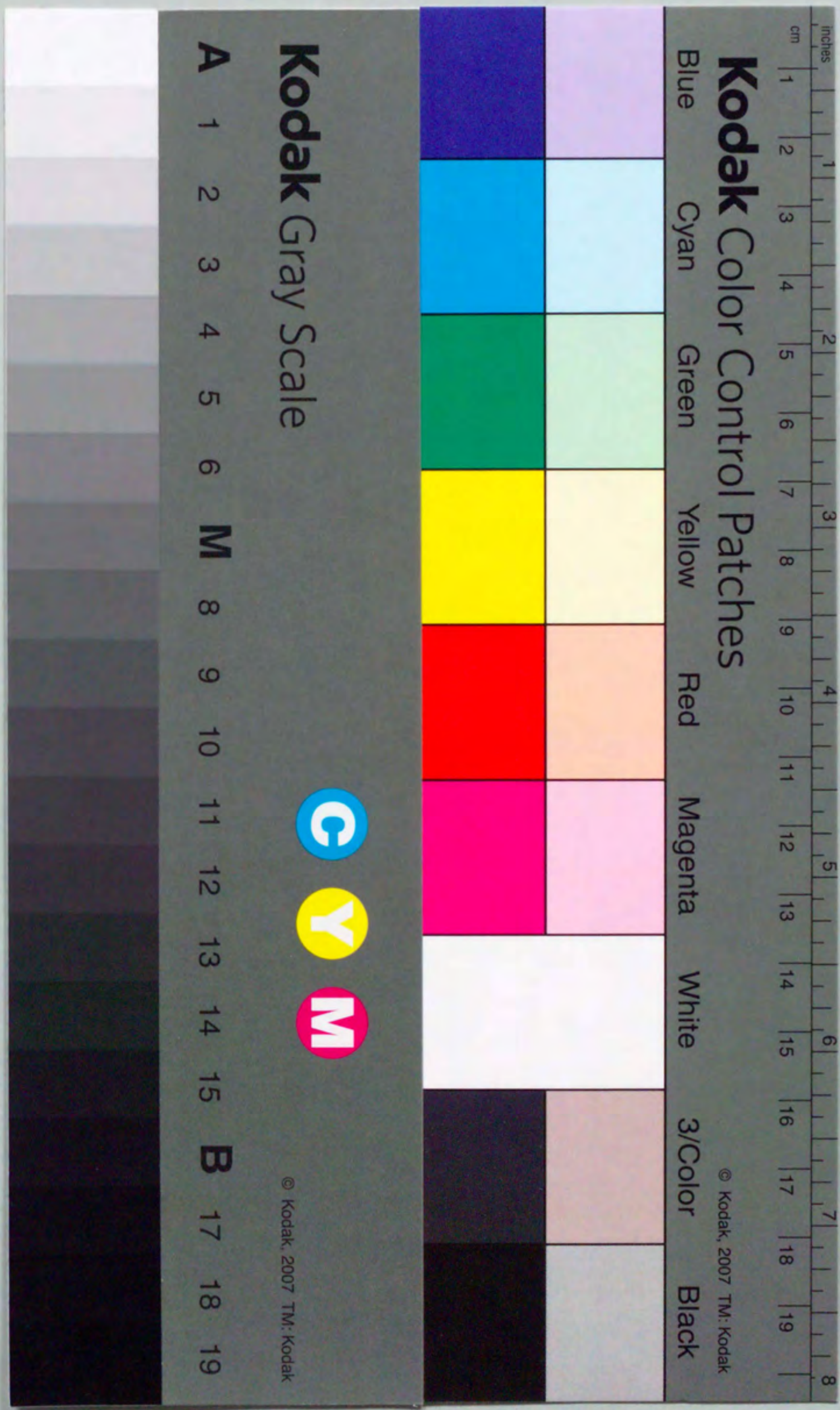
Kodak Color Control Patches
Blue
Cyan
Green
Yellow
Red
Magenta
White
3/Color
Black
© Kodak, 2007 TM: Kodak
Kodak Gray Scale
A 1 2 3 4 5 6 M 8 9 10 11 12 13 14 15 B 17 18 19
C Y M
© Kodak, 2007 TM: Kodak